

1
2
3
4
5
6
7
8
9
10
11
12
13
14
15
16
17
18
19
20
21
22
23

Article type : Article

Journal: Ecological Applications

Manuscript type: Articles

Running Head: Bayesian estuarine hypoxia forecasting

Advancing estuarine ecological forecasts: seasonal hypoxia in Chesapeake Bay

Donald Scavia^{1,*}, Isabella Bertani², Jeremy M. Testa³, Aaron J. Bever⁴, Joel D. Blomquist⁵,
Marjorie A.M. Friedrichs⁶, Lewis C. Linker⁷, Bruce D. Michael⁸, Rebecca R. Murphy², Gary W.
Shenk⁹

¹ School for Environment and Sustainability, University of Michigan, Ann Arbor, MI
USA 48103

² University of Maryland Center for Environmental Science, Chesapeake Bay Program
Office, Annapolis, MD USA 21403

³ Chesapeake Biological Laboratory, University of Maryland Center for Environmental
Science, Solomons, MD USA 20688

This is the author manuscript accepted for publication and has undergone full peer review but has not been through the copyediting, typesetting, pagination and proofreading process, which may lead to differences between this version and the [Version of Record](#). Please cite this article as [doi: 10.1002/EAP.2384](https://doi.org/10.1002/EAP.2384)

This article is protected by copyright. All rights reserved

24
25
26
27
28
29
30
31
32
33
34
35
36
37
38
39
40
41
42
43
44
45
46
47
48
49
50
51

⁴ ANCHOR QEA, LLC, San Francisco, CA USA 94111
⁵ Water Observing Systems Program, U.S. Geological Survey, Baltimore, MD USA 21228
⁶ Virginia Institute of Marine Science, William & Mary, Gloucester Point, VA USA 23062
⁷ U.S. EPA Chesapeake Bay Program Office, Annapolis, MD USA 21403
⁸ Department of Natural Resources, Annapolis, MD USA 21401
⁹ U.S. Geological Survey Chesapeake Bay Program Office, Annapolis, MD USA 21403

*Corresponding Author: scavia@umich.edu

Manuscript received 26 January 2021; revised 28 April 2021; accepted 26 May 2021.

ABSTRACT

Ecological forecasts are quantitative tools that can guide ecosystem management. The co-emergence of extensive environmental monitoring and quantitative frameworks allows for widespread development and continued improvement of ecological forecasting systems. We use a relatively simple estuarine hypoxia model to demonstrate advances in addressing some of the most critical challenges and opportunities of contemporary ecological forecasting, including predictive accuracy, uncertainty characterization, and management relevance. We explore the impacts of different combinations of forecast metrics, drivers, and driver time windows on predictive performance. We also incorporate multiple sets of state-variable observations from different sources and separately quantify model prediction error and measurement uncertainty through a flexible Bayesian hierarchical framework. Results illustrate the benefits of 1) adopting forecast metrics and drivers that strike an optimal balance between predictability and relevance to management, 2) incorporating multiple data sources in the calibration dataset to separate and propagate different sources of uncertainty, and 3) using the model in scenario mode to probabilistically evaluate the effects of alternative management decisions on future ecosystem state. In the Chesapeake Bay, the subject of this case study, we find that average summer or total

52 annual hypoxia metrics are more predictable than monthly metrics and that measurement error
53 represents an important source of uncertainty. Application of the model in scenario mode
54 suggests that absent watershed management actions over the past decades, long-term average
55 hypoxia would have increased by 7% compared to 1985. Conversely, the model projects that if
56 management goals currently in place to restore the Bay are met, long-term average hypoxia
57 would eventually decrease by 32% with respect to the mid-1980s.

58

59

60 **KEY WORDS:** Bayesian, Chesapeake Bay, Forecasts, Hypoxia

61

62 **INTRODUCTION**

63 Stakeholders, resource managers, and policy makers need to base their decisions on the best
64 available knowledge of how natural resources are expected to respond to environmental and
65 anthropogenic change. Making accurate and reliable quantitative ecological predictions is one of
66 the key challenges faced by contemporary applied ecology (Carpenter 2002; Evans et al. 2013;
67 Moquet et al. 2015). In response to this need, a growing number of efforts have advanced
68 ecological forecasting (Coreau et al. 2009; Luo et al. 2011; Payne et al. 2017; Ross et al. 2020).
69 Previously defined as “the process of predicting the state of ecosystems, ecosystem services, and
70 natural capital, with fully specified uncertainties” (Clark et al. 2001), ecological forecasts seek to
71 not only strengthen linkages between management questions and relevant research, but also to
72 advance scientific knowledge of mechanisms underlying ecosystem dynamics (Testa et al.
73 2017a; Dietze et al. 2018).

74 While forecasts of atmospheric conditions have long been a feature of climate science and
75 operational weather forecasting, ecological forecasts have been less frequently applied given the
76 challenges of modeling ecological systems and limitations of adequate data (e.g., Petchey et al.
77 2015). Nonetheless, the potential for ecological forecasts to guide and improve management
78 decisions has sparked interest beyond academic settings, with several government agencies
79 investing resources and supporting initiatives to explore its development and application. The
80 United States National Oceanographic and Atmospheric Administration (NOAA) has a long

81 history of both experimental and operational forecasts in areas such as harmful algal blooms,
82 hypoxia, fisheries, and pathogens (Valette-Silver and Scavia 2003; NOAA 2020), and other US
83 agencies have sponsored similar efforts (Bradford et al. 2020; NASA 2020). A recently launched
84 Ecological Forecasting Initiative represents the first broad effort to bring all these experiences
85 together and foster the development of an interdisciplinary forecasting community (EFI 2020).
86 Despite growing interest and an increasing number of applications, there is currently no broad
87 consensus on the ultimate predictability of ecological systems and the ability of models to
88 generate reliable predictions to inform policy (Beckage et al. 2011; Schindler and Hillborn
89 2015). This may be partly because most ecological forecasting efforts are relatively recent and
90 lack sufficiently long track records that build confidence. In addition, rigorous out-of-sample
91 forecast skill assessment is not always performed (Johnson-Bice et al. 2020) either because
92 forecasts are made over time frames (decades to centuries) that prevent timely comparisons with
93 observed data (Dietze et al. 2018) or because protocols are not in place for regular forecast
94 validation with new observations (White et al. 2019). Finally, although modeling approaches that
95 quantify multiple sources of uncertainty are becoming increasingly common (Harwood and
96 Stokes 2003; Clark 2005; Gimenez et al. 2014; Salon et al. 2019; Scavia et al. 2020c), a rigorous
97 treatment of uncertainty is often missing (Dietze et al. 2018). This may result in overly confident
98 forecasts that do not capture the full range of possible outcomes, thereby potentially leading to
99 inadequate preparedness and loss of trust in models when observations fall outside of
100 (underestimated) uncertainty bounds (Pappenberger and Beven 2006; Raftery 2016).

101 Models of oxygen dynamics date back a century or more (e.g., Streeter and Phelps 1925) and
102 forecasts of hypoxia extent are perhaps one of the most established and mature examples of
103 routine and operational ecological forecasts. Such forecasts for the Gulf of Mexico date back
104 almost two decades (Scavia et al. 2003, 2017), followed in more recent years by similar efforts in
105 other systems, such as the Chesapeake Bay (Scavia et al. 2006; Testa et al. 2017a; VIMS 2020b;
106 Bever et al. 2021), Lake Erie (NOAA GLERL 2020), and the Neuse River Estuary (Katin et al.
107 2019; North Carolina Sea Grant 2020). Among these, the Chesapeake Bay has a 14-year
108 transparent record of ecological forecast performance based on regular comparisons of
109 predictions with out-of-sample observations (e.g., Scavia and Bertani 2020) and model validation
110 (Evans and Scavia 2011). Since 2007, a statistical model that incorporates simple biophysical
111 processes has been used to forecast mid-summer hypoxic volume (HV) in the Chesapeake Bay as

112 a function of total nitrogen (TN) loads from the largest tributary to the Bay (Susquehanna River)
113 (Scavia et al. 2006). Each year, the model's forecast is assessed at the end of the season by
114 comparing it to hypoxia observations made by monitoring agencies (Maryland DNR 2020;
115 Scavia and Bertani 2020). Informed by this continuous validation and assessment process, the
116 model has been revised over the years with a focus on improving performance and uncertainty
117 characterization (Stow and Scavia 2009; Liu et al. 2011). Testa et al. (2017a) showed that these
118 forecasts contributed substantially to public awareness and support for management actions in
119 the Chesapeake Bay, in addition to helping advance fundamental understanding of ecological
120 processes driving oxygen depletion in estuarine settings.

121 In this work, we build on the Chesapeake Bay hypoxia case study and present an enhanced
122 version of the forecasting model that addresses some of the most critical challenges,
123 opportunities, and best practices of contemporary ecological forecasting. These include
124 identifying predictors and metrics of ecosystem state that improve model performance and
125 management relevance, explicitly accounting for and propagating multiple sources of
126 uncertainty, evaluating forecasting performance through hindcasting, and applying the model to
127 answer management questions (Dietze et al. 2018; Harris et al. 2018; White et al. 2019; Carey et
128 al. 2021). Guided by recent appreciation for the spatial distribution of nutrient sources that affect
129 the Bay's water quality, how loads have changed over time, and the complex intra-annual
130 variability in hypoxia, we explore how model performance changes when different combinations
131 of HV metrics, TN load sources, and TN load time windows are used as calibration inputs. We
132 also take advantage of the model's flexible Bayesian framework to better characterize
133 uncertainty by including multiple data sources (i.e., multiple sets of HV estimates) during
134 calibration through a hierarchical approach that separates model prediction error and HV
135 measurement error. Finally, we validate the model through hindcasting and showcase the use of
136 the model for scenarios by predicting hypoxic conditions (with associated probability
137 distributions) under alternative nutrient management scenarios routinely evaluated by the
138 Chesapeake Bay Program (CBP), the Partnership that leads restoration efforts in the Bay.

139

140 **METHODS**

141 **Historical context and management background**

142 Like many coastal ecosystems worldwide, water quality of the Chesapeake Bay, the largest
143 estuary in the continental US, declined as a result of human activity over at least the last century
144 (Kemp et al. 2005). Loss of submerged aquatic vegetation (Kemp et al. 2005), altered benthic
145 macroinvertebrate production (Sturdivant et al. 2013), and extensive hypoxia (e.g., Hagy et al.
146 2004) are among the water quality impairments caused by elevated nutrient inputs, land use
147 changes, and resource extraction. Extensive efforts have been in place to reduce nitrogen (*N*),
148 phosphorus (*P*), and sediment (*S*) inputs since the 1980s, with the goal of improving water
149 quality and reducing hypoxia (Linker et al. 2013; Shenk and Linker 2013). The United States
150 Environmental Protection Agency (US EPA), working together with federal, state, local, and
151 non-governmental partners, established a Total Maximum Daily Load (TMDL) in 2010 for *N*, *P*,
152 and *S* (US EPA 2010). To meet the TMDL load reduction targets, state and local governments
153 are responsible for developing Watershed Implementation Plans (WIPs) that describe needed
154 management practices. Coincident with these efforts, which have also included point source
155 decreases (Ator et al. 2020) and reductions in atmospheric nitrogen deposition (Eshleman et al.
156 2013; Da et al. 2018), water clarity and dissolved oxygen (DO) concentrations have improved
157 some (Zhang et al. 2018) and submerged aquatic vegetation has expanded in some regions
158 (Gurbisz and Kemp 2014; Lefcheck et al. 2018). However, progress has been slow (Boesch
159 2006) and currently less than half of the Bay area meets all water quality goals (Zhang et al.
160 2018).

161 One of the primary TMDL goals is raising DO concentrations to levels suitable for upper trophic
162 levels (e.g., invertebrates, finfish). Low oxygen concentrations have contributed to decreased fish
163 habitat, catch per unit effort (Buchheister et al. 2013), and blue crab harvests (Mistiaen et al.
164 2003), as well as reductions in production of benthic macroinvertebrates (Sturdivant et al. 2014)
165 that serve as forage for many demersal fish. Although there is some evidence for recent
166 improvements in DO in certain periods or when considering specific metrics (Murphy et al.
167 2011; Zhang et al. 2018), the overall annual volume of water with oxygen less than 2 mg/L (~63
168 mM) has changed little over the past 3-4 decades (Testa et al. 2018; Bever et al. 2018).

169 In support of nutrient control efforts, the CBP uses complex airshed, watershed, and water
170 quality models (US EPA 2010) to determine oxygen concentration targets (Irby and Friedrichs
171 2019), but other predictive models have been used to both forecast and study oxygen dynamics

172 (e.g., Testa et al. 2014; Irby et al. 2016, 2018; Da et al. 2018; Du et al. 2018; Moriarty et al.
173 2020), including the model presented here (Scavia et al. 2006).

174

175 **Model overview**

176 The model used here is an adaptation of the Streeter-Phelps model that simulates DO depletion
177 in rivers downstream from a point source of organic matter (Streeter and Phelps 1925). It has
178 been applied extensively to rivers and estuaries (Chapra 1997), as well as to the northern Gulf of
179 Mexico (Scavia et al. 2003, 2004, 2006, 2017, 2020b) and the Chesapeake Bay (Scavia et al.
180 2006, 2019; Liu et al. 2011; Evans and Scavia 2011).

181 The model simulates subpycnocline DO concentration profiles along the mainstem of the
182 Chesapeake Bay via subpycnocline net advection, organic matter decomposition and oxygen
183 consumption, and oxygen flux from the surface layer. Assuming a correspondence between the
184 measured extent of summer hypoxia and that which would be achieved at steady state, the steady
185 state solution to the model is:

$$186 \quad DO = DO_s - \frac{k_d BOD_u F}{k_r - k_d} \left(e^{-k_d \frac{x}{v}} - e^{-k_r \frac{x}{v}} \right) - D_i e^{-k_r \frac{x}{v}} \quad \text{Eq. 1}$$

187 where DO = dissolved oxygen (mg/L), DO_s = oxygen saturation (mg/L), k_d = organic matter
188 decay coefficient (1/day), k_r = reaeration coefficient (1/day), BOD_u = initial organic matter
189 (mg/L), x = upstream distance (km), F = fraction of organic matter sinking below the pycnocline
190 (unitless), D_i = initial oxygen deficit (mg/L), and v = net advection (km/day). Because the
191 reaeration coefficient k_r is known to vary with distance down estuary x , the model calculates $k_r =$
192 $b_x K$, where b_x takes on different values over the length of the estuary that approximate the known
193 spatial variation in k_r (Scavia et al. 2006; Evans and Scavia 2011) and K is a unitless scaling
194 parameter estimated by the model. While v represents river advection in the original Streeter-
195 Phelps formulation, here it is a parameterization of the combined effects of horizontal transport
196 and all ecological processes resulting in subsequent settling of organic matter from the surface.
197 Therefore, it is a bulk parameter with no simple physical analog.

198 Nitrogen load is a surrogate for organic matter deposited below the pycnocline at the model
199 origin (220 km down Bay from the Susquehanna River mouth), with model distance following

200 the up-estuary flow of bottom water. Specifically, nitrogen load is converted to organic carbon
201 (C) via the Redfield C:N ratio (106:16 or 5.67 g C/g N), and then converted to BOD_u via the
202 respiration ratio O₂:C (0.9, or 2.4 g O₂/g C) (Scavia et al. 2006). In the original model, organic
203 matter loading was assumed proportional to Jan-May Susquehanna River TN load; in this study
204 additional load sources and time windows were tested (see below).

205 The Bay mainstem is divided into 137 1-km long segments and Eq. 1 is applied to estimate the
206 steady state subpycnocline DO concentration at each segment j and in each year i (DO _{ij}). The
207 overall length of the model-predicted hypoxic region in each year i (L_i) is then calculated by
208 summing the lengths (l_{ij}) of all segments where DO _{ij} is less than 2 mg/L (Eqs. 2 and 3) and HV
209 (V_i) is calculated from L_i using an empirical relationship (Eq. 4) derived from Chesapeake Bay
210 measurements (Scavia et al. 2006):

$$211 \quad L_i = \sum_{j=1}^{137} l_{ij} w_{ij} \quad \text{Eq. 2}$$

$$212 \quad w_{ij} = \begin{cases} 1, & DO_{ij} < 2 \\ 0, & DO_{ij} \geq 2 \end{cases} \quad \text{Eq. 3}$$

$$213 \quad V_i = 0.000391 \times L_i^2 \quad \text{Eq. 4}$$

214 Other assumptions include: transport results from advection rather than longitudinal dispersion,
215 subpycnocline oxygen consumption can be modeled as a first-order process proportional to
216 organic matter concentration, oxygen flux across the pycnocline can be modeled as a first-order
217 process proportional to the difference between surface and bottom layer oxygen concentrations,
218 and subpycnocline organic matter oxygen demand is proportional to TN load. Tests of these
219 assumptions, as well as calibration to average July subpycnocline oxygen concentration profiles
220 and HVs from 1950 to 2003, have been described elsewhere (Scavia et al. 2006). Annual
221 forecasts provided each spring since 2007 were shown to be rather robust (Scavia and Bertani
222 2020; Testa et al. 2017a).

223

224 **Nitrogen load sources and time frames**

225 We assembled TN loads from major tributaries and point sources downstream of the tributary
226 monitoring stations (Figs. 1 and Appendix S1: Fig. S1) and tested various combinations of load

227 sources and time frames as model drivers. Monthly TN loads estimated from 1985-2018 at
228 stations located near the head of tide of nine major tributaries (Susquehanna, Potomac, James,
229 Rappahannock, Appomattox, Pamunkey, Mattaponi, Patuxent, and Choptank) were from the
230 United States Geological Survey (<https://doi.org/10.5066/F7RR1X68>). Estimates of TN loads
231 from point sources located downstream of these tributaries were from the CBP (Chesapeake Bay
232 Program 2017). Monthly point source loads are based on wastewater facility monthly flow and
233 constituent concentration data submitted by the jurisdictions to the Integrated Compliance
234 Information System National Pollutant Discharge Elimination System (ICIS-NPDES) and
235 subsequently reviewed and quality checked by the CBP. On average, these nine tributaries and
236 point sources make up approximately 77% of the 1990-2018 average annual TN load (calculated
237 from <https://www.chesapeakeprogress.com/?/clean-water/water-quality>). We explored model
238 performance using each of the following combinations of sources: Susquehanna alone, Potomac
239 alone, Susquehanna + Potomac, Susquehanna + Potomac + point sources, all nine major
240 tributaries, all nine major tributaries + point sources.

241 To evaluate the impact of different loading time frames on model performance, for each of the
242 load source combinations described above, we calculated loads from the preceding year's
243 October and each succeeding month through April (e.g., Oct-Apr, Nov-Apr, Dec-Apr, Jan-Apr,
244 Feb-Apr, Mar-Apr, Apr), and then similar sequences through May, June, and July. We first
245 screened candidate load windows by calculating the Pearson's correlation coefficient between
246 HV metrics and different combinations of TN load windows \times TN load sources. Initial
247 explorations revealed that regardless of the TN load sources considered, load time windows
248 ending in April or earlier never improved correlations compared to time windows that considered
249 loads through May or later, so we only included time windows ending in May or later. In
250 addition, correlations between HV metrics and TN loads in the Oct-Jul window were generally
251 comparable to, or worse than, those obtained with Oct-May and Oct-Jun. Because of that, and
252 considering that hypoxia forecasts are typically released in early June (i.e., before the July loads
253 can be reliably predicted), we focused model calibration exercises on all possible sequential
254 combinations of months in the Oct-May and Oct-Jun time windows.

255

256 **Hypoxic volume metrics**

257 As part of the CBP's long-term Water Quality Monitoring Program, Virginia and Maryland state
258 agencies and partners have collected vertical profiles of DO since 1984 and made the data
259 available through the CBP's online data server (Chesapeake Bay Program 2020). Roughly 30-60
260 stations in the mainstem portion of the Bay are sampled semi-monthly in June through August
261 and monthly throughout the remainder of the year, with vertical profiles collected at about 1-2 m
262 vertical resolution. These data have been used by numerous groups to estimate the extent of
263 hypoxia in the Chesapeake Bay (Bever et al. 2013, 2018; Zhou et al. 2014; Hagy et al. 2004;
264 Murphy et al. 2011).

265 Previous versions of the model were calibrated to average July HV estimated through
266 interpolation of DO measurements from a subset of the mainstem stations mentioned above by
267 Hagy et al. (2004) and by Murphy et al. (2011) in more recent years (Scavia et al. 2019). The
268 month of July was originally selected because that is when HV often reaches its seasonal
269 maximum. However, retrospective assessments of forecast performance revealed consistent
270 overprediction of July HV in years characterized by anomalous weather events (Testa et al.
271 2017a). In addition to that, different metrics may capture different aspects of an ecosystem's
272 status and metrics other than the seasonal maximum HV may be more relevant to stakeholders
273 and decision makers depending on the specific ecological management target. For example,
274 managers interested in assessing spawning habitat availability for a benthic species that tends to
275 spawn in June would be more interested in average June HV. On the other hand, total annual HV
276 may be the preferred metric when tracking watershed management progress over time, because it
277 may be less sensitive to year-specific transient weather events and may better capture the
278 cumulative effects of changes in nutrient loads over time. One of the goals of our analysis was
279 thus to assess how model performance changed when different HV metrics were used as
280 calibration endpoint to 1) identify which metrics may lead to improved forecasting performance
281 and 2) provide stakeholders and managers with useful information on each metric's
282 predictability.

283 To compare model performance for different combinations of HV metrics, load sources, and load
284 time frames while maintaining an interpolation method consistent with previous model versions,
285 we used the updated time series (1985-2018) of HV estimates generated following Murphy et al.
286 (2011). Murphy et al. (2011) apply two-dimensional (depth-length) ordinary kriging to DO
287 observations collected during semi-monthly cruises at 21 stations along the main channel of the

288 Bay. The interpolated DO profile estimated along the main channel for each cruise is assumed to
289 remain constant across the mainstem and is extended laterally to estimate cruise-specific HV
290 based on previously published cross-sectional volumes.

291 We tested six different HV metrics in the model's calibration (Figs. 2 and Appendix S1: Fig. S2):
292 average of the two cruise-specific HVs for each month for June through September (km^3),
293 average summer (defined as June-September) HV (km^3), and total annual HV ($\text{km}^3 \cdot \text{days}$). In
294 cases when only a single cruise was available in a month (typically in September and
295 sporadically in other months), that cruise's value was taken as the monthly HV. Total annual HV
296 was estimated by multiplying each cruise-specific HV by the number of days until the following
297 cruise and then summing these values over each year (Bever et al. 2013).

298

299 **Hypoxic volume interpolation methods**

300 We considered two additional sets of HV estimates to investigate the influence of the
301 interpolation methods on variability in HV estimates and model predictive uncertainty. We note
302 that we use the terms "variability" and "model predictive uncertainty" to indicate, respectively,
303 the range of variation of an outcome (e.g., HV) around its mean and the stochastic error
304 component that estimates that variation within a model (e.g., the residual error term in a
305 regression model) (Gelman and Hill 2007; Hofman et al. 2020). The different sets of HV
306 estimates were generated using different subsets of DO profile stations as well as different
307 interpolation methods. Zhou et al. (2014) performed universal kriging on cruise-specific DO
308 profiles from approximately 40 stations located across the mainstem of the Bay. Bever et al.
309 (2018) used the CBP volumetric inverse distance-squared interpolator (US EPA 2003) with DO
310 profiles from a subset of 13 stations along the mainstem and in the lower Potomac River.
311 Differences in cruise-specific HVs across these three methods (hereafter referred to as Murphy,
312 Zhou, and Bever) are expected as a result of several factors, including differences in the
313 interpolation approaches and relevant methodological choices (e.g., DO profile stations used),
314 the bathymetry used in the interpolations, and the spatial extent over which interpolation was
315 carried out.

316 Zhou et al. (2014) and Murphy et al. (2011) limited their spatial extent to the mainstem, while
317 Bever et al. (2018) extended interpolations to the tributaries. To adjust for these differences

318 while preserving the individual inter-annual variability, we scaled Murphy and Zhou HVs to
319 Bever's using the average long-term ratio of mainstem-only HV to Bay-wide HV simulated by
320 the CBP Water Quality and Sediment Transport Model (WQSTM). A comparison with long-
321 term ratios of mainstem-only HV to Bay-wide HV calculated using HVs estimated by the CBP
322 volumetric interpolator over the period 1985-2013 indicated that ratios estimated by the CBP
323 WQSTM and the CBP interpolator are largely comparable (Appendix S1: Fig. S3). Because
324 average ratios calculated for individual months and total annual HV did not differ substantially,
325 we applied the total annual HV ratios to Zhou's and Murphy's monthly, average summer, and
326 total annual HV metrics.

327 To quantify uncertainty due to HV estimation error and model prediction error separately, we
328 used a hierarchical modeling approach to expand the original model formulation and
329 simultaneously calibrate the model to the three sets of HV estimates (Obenour et al. 2014). The
330 three individual HV estimates in each year i are modeled as arising from a normal distribution
331 with mean y_i and standard deviation σ_{est} (Eq. 5). In this formulation, y_i represents the true,
332 unknown HV in year i and is itself modeled as arising from a normal distribution with mean
333 equal to the deterministic model prediction in year i as defined in Eqs. 1 and 4 (V_i) and standard
334 deviation σ_{res} (Eq. 6):

$$335 \text{vol}_{i,j} \sim \text{Normal}(y_i, \sigma_{est}^2) \quad \text{Eq. 5}$$

$$336 y_i \sim \text{Normal}(V_i, \sigma_{res}^2) \quad \text{Eq. 6}$$

337 where $\text{vol}_{i,j}$ represents the HV estimate from method j (with $j=1$ for Murphy, $j=2$ for Bever, and
338 $j=3$ for Zhou) in year i and the two stochastic terms σ_{est} and σ_{res} represent uncertainty deriving
339 from HV estimation error and model prediction error, respectively.

340

341 **Calibration and model skill assessment**

342 The original model (Scavia et al. 2006) was a Monte Carlo implementation that accommodated
343 potential variation in the bulk parameter v . It was subsequently reformulated within a Bayesian
344 framework (Evans and Scavia 2011; Liu et al. 2011) to account for uncertainty in additional
345 parameters. In the present study, the model was calibrated under the range of conditions

346 described above using Bayesian fitting conducted with the software WinBUGS version 1.4.3
347 (Lunn et al. 2000; Gelman and Hill 2007) interfaced with R version 3.5.2 (R Core Team 2018)
348 through the package R2WinBUGS version 2.1-21 (Sturtz et al. 2005). All model parameters
349 were kept constant across years. The two parameters quantifying sources of uncertainty (σ_{est} and
350 σ_{res}) are represented as precisions in WinBUGS (τ_{est} and τ_{res} , where $\tau = 1/\sigma^2$) and were assigned
351 weak priors: $\tau_{\text{est}}, \tau_{\text{res}} \sim \text{Gamma}(0.001, 0.001)$, while all other parameters were given the same
352 priors used in the most recent model applications: $K \sim \text{Normal}(0.6, 0.2)I[0, 1]$; $F \sim \text{Normal}(0.5,$
353 $0.5) I[0, 1]$; $k_d \sim \text{Normal}(0.11, 0.05)I[0,]$; and $v \sim \text{Normal}(2.5, 0.77)I[0,]$, where the Gamma
354 distribution is defined by the shape and rate parameters, the Normal distribution is defined by the
355 mean and standard deviation, and ‘I[]’ denotes censoring to restrict values above 0 (I[0,]) or
356 between 0 and 1 (I[0, 1]) (Evans and Scavia 2011; Liu et al. 2011). We ran four Markov Chain
357 Monte Carlo chains with 5,000 iterations each and checked convergence by ensuring that $\hat{R} < 1.1$
358 for all model parameters. We assessed how model performance changed when using multiple
359 sets of HV estimates and different combinations of HV metrics, TN load sources, and TN load
360 time windows using a combination of several metrics: the Nash-Sutcliffe Efficiency (NSE), the
361 square of the correlation coefficient between observed and predicted values (r^2), the root mean
362 square error (RMSE), the mean absolute error (MAE), and the residual standard error (RSTDE)
363 (see Appendix S1 for a description of how each metric was calculated). Specifically, we
364 evaluated all metrics simultaneously and assessed whether all metrics agreed in indicating which
365 model performed best. By ensuring a high level of agreement among different metrics we aimed
366 at providing a more comprehensive and robust assessment of the models’ performance. When
367 multiple sets of HV estimates were used in model calibration, all individual HV estimates from
368 the different sets were used to calculate model performance metrics.

369 For the models exhibiting the best predictive performance according to the metrics defined
370 above, we also computed the coverage of the 95% prediction intervals (i.e., the fraction of the
371 observations that fell within the intervals) and the Continuous Ranked Probability Score (CRPS)
372 (Matheson and Winkler 1976). The CRPS quantifies the error between the cumulative
373 distribution function of a model’s prediction and that of the corresponding observed value,
374 thereby providing an assessment of the calibration and sharpness of the predictive distributions
375 (Gneiting and Katzfuss 2014). We used the R package scoringRules version 1.0.1 (Jordan et al.
376 2019) to calculate a CRPS value for each observation and then obtained a mean CRPS value for

377 each model by averaging across all observations. We then calculated a CRPS skill score (Eq. 7)
378 by comparing each model's CRPS ($CRPS_{model}$) with that of a respective benchmark null model
379 ($CRPS_{benchmark}$) that does not have TN load as the predictor and thereby essentially
380 corresponds to a constant-only model that predicts HV simply based on the historical long-term
381 average (Pappenberger et al. 2015; Thomas et al. 2019):

$$382 \quad CRPS \text{ skill score} = 1 - \frac{CRPS_{model}}{CRPS_{benchmark}} \quad \text{Eq. 7}$$

383 Because lower CRPS values indicate better performance, with zero corresponding to a perfect
384 prediction, a CRPS skill score of 1 indicates a perfect prediction, values above zero indicate that
385 a model is more skillful than its respective benchmark null model, and conversely values below
386 zero indicate that a model performs worse than the benchmark.

387 **Response curves and scenarios**

388 Response curves were developed for the two best performing models by generating HV
389 predictions, with 95% credible and prediction intervals, for a range of TN loads. The response
390 curves were then used to estimate HVs for a set of alternative management scenarios routinely
391 evaluated by the CBP:

- 392 • **1985 FN and 2018 FN:** Obtained by summing flow-normalized loads from all nine
393 tributaries plus point sources in 1985 and 2018, respectively. Flow normalization (Hirsch et
394 al. 2010) removes the influence of year-to-year variability in river flow, thereby providing
395 an estimate of the amount of change in loads between 1985 and 2018 that may be attributed
396 to changing nutrient sources, management actions, and other factors.
- 397 • **2020 No Action:** Obtained by multiplying each tributary's 1985 flow-normalized load by
398 the ratio of 2020 No Action/1985 Progress Real Air scenario loads estimated for that
399 tributary's sub-watershed by the CBP partnership's watershed model CAST (Chesapeake
400 Bay Program 2017). Tributary loads were then summed together with point sources from the
401 CAST 2020 No Action scenario. The 2020 No Action scenario estimates the long-term
402 average loads expected given a constant 2020 land use, human and livestock populations,
403 and cropping systems, but with management practices, point sources, septic loads, and
404 atmospheric deposition set as if no actions had been taken to control nutrients since 1985.

405 The 1985 Progress Real Air scenario estimates the long-term average loads expected from
406 the watershed at each monitoring station given a constant 1985 land use, management
407 practices, point sources, septic loads, cropping systems, livestock, and nutrient inputs of
408 fertilizers, manure, N fixation, and atmospheric deposition.

- 409 • **WIP3 Planning Targets:** Obtained by multiplying each tributary's 2018 flow-normalized
410 load by the ratio of Phase 3 Watershed Implementation Plan (WIP3) Planning Targets/2018
411 Progress Real Air scenario loads. Tributary loads were then summed together with point
412 sources from the CAST WIP3 scenario. The WIP3 Planning Targets represent loads
413 consistent with the Bay's TMDL (US EPA 2010) that are expected to achieve target water
414 quality goals.
- 415 • **WIP3 Actual:** In some cases, the WIP3s submitted by the states did not meet the WIP3
416 Planning Targets. WIP3 Actual was obtained by multiplying each tributary's 2018 flow-
417 normalized load by the ratio of the actual WIP3 plans submitted by the states/2018 Progress
418 Real Air scenario loads estimated by CAST. Tributary loads were then summed together
419 with point sources from the CAST WIP3 Actual scenario. The WIP3 Actual scenario
420 estimates the long-term average loads expected if the WIP3s submitted by the states are
421 completed, using modeled 2025 land use and population conditions. The 2018 Progress Real
422 Air scenario is defined similarly to the 1985 Progress Real Air scenario defined above.

423

424 RESULTS

425 Total nitrogen loads and hypoxic volume metrics

426 Annual TN loads are dominated by the Susquehanna and Potomac rivers, followed by point
427 sources that enter below the monitoring stations (Fig. 1). There was considerable inter-annual
428 variability driven largely by precipitation. Highest loads occurred in especially wet years (e.g.,
429 2003, 2004, 2011) and lowest loads in drier years (e.g., 1999-2002). Loads were typically highest
430 in March and April, lowest in July and August, and most variable in September (Appendix S1:
431 Fig. S1).

432 There was also substantial inter-annual variability in HV. The three interpolation methods
433 showed relatively coherent patterns for total annual HV, summer average HV, and most of the

434 individual months (Figs. 2 and Appendix S1: Fig. S2 and Table S1), with particularly large HV
435 in 1998, 2003, and 2001, and relatively smaller volumes in 2001, 2002, and 2012. When
436 averaged across the three sets of estimates, the smallest annual HV occurred in 2002 (557 ± 30
437 $\text{km}^3 \cdot \text{days}$) and the largest in 2003 ($1235 \pm 240 \text{ km}^3 \cdot \text{days}$). In most years HV peaked in July and
438 declined between August and September, although there was substantial inter-annual seasonal
439 variability and in some years the largest HVs occurred in June or August. The largest monthly
440 HV was in July 2011. Using the coefficient of variation as an estimate of inter-annual variability,
441 all three estimates exhibited substantially higher inter-annual variability in monthly HVs
442 compared to summer average and total annual HV (Appendix S1: Table S1).

443

444 **Model calibration**

445 Based on general agreement among the performance metrics, the best fits (i.e., highest NSE,
446 highest r^2 , lowest RMSE, and lowest MAE) for total annual, summer average, and August HV
447 were achieved when driven with Jan-Jun loads from all tributaries plus point sources (Table 1;
448 Fig. 3). The June and July HV best fits were obtained with slightly different TN load sources and
449 periods (Table 1), but their second-best models were also based on loads from all tributaries and
450 point sources and were virtually indistinguishable from the best models' performance.

451 Interestingly, models calibrated to only Susquehanna loads never ranked among the ten best-
452 performing models for any of the HV metrics considered here. As an example, based on NSE the
453 best performing models driven by TN loads from only the Susquehanna River explained 28%
454 and 23% of the inter-annual variability in total annual and average July HV, respectively,
455 compared to 52% and 29% obtained when using loads from all tributaries and point sources
456 (Table 1). All models exhibited a CRPS skill score > 0 , indicating that all models represented an
457 improvement in performance compared to the respective null models, and the percentage of
458 observations that fell within the 95% prediction intervals ranged between 94% and 100% (Table
459 1).

460 The highest model performances were obtained for average summer and total annual HV (Table
461 1). The monthly HV models performed better earlier in the season (e.g., June and July) compared
462 to late summer (e.g., August and September), and the load time frames tested here had no
463 predictive power for September HV.

464 To more rigorously assess the performance of the overall best model (i.e., the one calibrated to
465 total annual HV and driven by Jan-Jun loads from all tributaries and point sources), we generated
466 blind forecasts for the years when regular forecasts were made (i.e., starting in 2007). To forecast
467 each year, we calibrated the model using data up to the preceding year. This provides a more
468 realistic estimate of how the model would perform when predicting outside of the calibration
469 dataset. When run in this blind forecast mode, 100% of the left-out, post-2006 observations fell
470 within the 95% prediction intervals and the CRPS skill score was equal to 0.14, indicating an
471 improvement in performance compared to a corresponding null model run in blind forecast
472 mode. Values of NSE indicated that the blind forecast total annual HV model explained 47% of
473 the variability in HV when considering all years in the 2007-2018 window, and 58% of the
474 variability in HV when excluding three years characterized by mid-summer disruptive weather
475 events (2007, 2014, and 2018; Fig. 2). For comparison, when calibrated to only Susquehanna TN
476 loads, the model explained 23% and 27% of the variability in total annual HV across all years
477 and “normal” weather years, respectively.

478

479 **Sources of uncertainty**

480 When calibrating the best-performing models (i.e., average summer and total annual HV driven
481 by Jan-Jun loads from all tributaries plus point sources) to three sets of HV estimates
482 simultaneously, predictive performance (average summer: NSE = 0.39, $r^2 = 0.52$, RMSE = 1.11,
483 MAE = 0.89; total annual: NSE = 0.50, $r^2 = 0.60$, RMSE = 136, MAE = 107) was comparable to
484 that of the models calibrated using the same inputs but one set of HV estimates only (Table 1).
485 Model prediction error (σ_{est}) and HV estimation error (σ_{res}) were similar, suggesting that the two
486 sources of uncertainty are of comparable magnitude (Appendix S1: Table S2). The 95%
487 prediction intervals accounting for parameter uncertainty, model prediction error, and HV
488 estimation error contained the corresponding observed values 97% of the times for both models,
489 and were on average 20% wider than those accounting for only parameter uncertainty and model
490 prediction error (Fig. 4). The CRPS was equal to 75 km³ (total annual HV) and 0.63 km³
491 (average summer HV) while the CRPS skill score was equal to 0.26 (average summer HV) and
492 0.34 (total annual HV), indicating that the models performed better than the corresponding
493 benchmark null models. Although model residuals did not show a clear trend over time, the ratio

494 of total annual or summer average HV over the Jan-Jun TN load exhibited a significant positive
495 trend using the two sets of HV estimates (Murphy and Bever) with complete records over 1985-
496 2018 (Appendix S1: Fig. S4).

497

498 **Response curves and scenarios**

499 Parameters from the best models were used to construct HV-load response curves for summer
500 average and total annual HV (Fig. 4). The best-estimate curve indicates that, based on flow-
501 normalized loads, total annual HV declined on average from 930 km³*days (95% credible
502 interval, or CI: 840-1005 km³*days) to 770 km³*days (95% CI: 640-870 km³*days) between
503 1985 and 2018 (Fig. 4a and Appendix S1: Table S2). These estimates are not meant to
504 characterize HV in a specific year, but rather to quantify the change in HV predicted by the
505 model between two given time periods over the long-term after averaging out the influence of
506 inter-annual variability in TN loads due primarily to freshwater flow variability.

507 We also explored load reductions associated with specific management scenarios generated by
508 the CBP Partnership's watershed model CAST. The results suggest that had there been no point
509 or nonpoint source management actions, long-term average HV would have increased to 995
510 km³*days (95% CI: 910-1085 km³*days) by 2020. The model also projects that if the TMDL is
511 reached, long-term average HV would decrease to 635 km³*days (95% CI: 440-785 km³*days),
512 or to 660 km³*days (95% CI: 480-785 km³*days) if the WIP3 Actual reductions are reached.
513 This TMDL-based HV reduction represents 18% (95% CI: 10-32%) and 32% (95% CI: 22-49%)
514 reduction from 2018 and 1985 flow-normalized conditions, respectively. Similar results were
515 found for summer average HV (Appendix S1: Table S2).

516 For both total annual and summer average HV, TN load changes occurring at relatively high
517 loads produce relatively small changes in HV. But, as loads decrease the curve's slope becomes
518 steeper and the HV change per unit TN load increases, suggesting HV reductions may become
519 more responsive as loads continue to decrease.

520

521 **DISCUSSION**

522 **Predictability of different HV metrics** - Hypoxic extent metrics used for forecasts, scenarios,
523 and reporting across several systems have often been estimates of summer maximum volume or
524 area (e.g., Liu et al. 2011; Scavia et al. 2003, 2006, 2016, 2017; Testa et al. 2017a; Obenour et al.
525 2012, 2015; Rucinski et al. 2016; Bocaniov and Scavia 2016; Zhang et al. 2016; but see Katin et
526 al. 2019; Del Giudice et al. 2020; Ross et al. 2020). However, these maxima are not necessarily
527 representative of year-long conditions. For example, years with particularly large July HV, the
528 metric historically used to forecast hypoxia in the Chesapeake Bay, do not always exhibit
529 comparably large total annual HV and vice versa (Fig. 2; Bever et al. 2013; VIMS 2020b). Our
530 results showed that summer average and total annual HV are considerably easier to predict than
531 monthly HV (Table 1). This is largely because short-term meteorological events that increase
532 vertical mixing and lateral advection of bottom water can temporarily decrease HV (Goodrich et
533 al. 1987; Scully 2010a; Testa et al. 2017b). While these HV disruptions are often relatively short-
534 lived, they increase variability at monthly scales and may lead to substantial overprediction on
535 short time scales (Testa et al. 2017a). Similar disruptions of seasonal hypoxia occur in other
536 systems (Turner et al. 2012; Bocaniov and Scavia 2016), leading to either incorporate weather-
537 related drivers or to shift to hypoxia metrics that better integrate conditions throughout the year
538 (Bever et al. 2013, 2018; Feng et al. 2012; Obenour et al. 2015; Matli et al. 2018, 2020).

539 In addition to being less sensitive to variability caused by episodic weather events, total annual
540 HV better captures cumulative effects of year-to-year variability in nutrient loads, as illustrated
541 by the largest improvement in performance when relating this metric to a more comprehensive
542 estimate of total watershed loads (Table 1). Annual HV also has the benefit of incorporating
543 climate change effects because it combines hypoxic volume and duration into one metric without
544 being biased by climate-driven shifts in the timing or location of hypoxia (Irby et al. 2018). By
545 representing a more integrated, annual-scale estimate of oxygen depletion, total annual HV may
546 also capture a broader measure of living resource habitat limitation over the annual cycle.

547 However, monthly forecasts might be more informative if they capture more temporally dynamic
548 representations of hypoxia severity within a year. Given the wide range of oxygen vulnerability
549 among marine species (e.g., Vaquer-Sunyer and Duarte 2008), forecasts that quantify periods of
550 both low and high hypoxia severity during a year may allow for more species-specific
551 quantification of potential habitat loss and physiological stress. For example, many benthic
552 invertebrates, which are an important forage base for finfish communities, can tolerate some

553 degree of hypoxia (e.g., Modig and Olafsson 1998), while more severe hypoxia has more
554 widespread ecosystem effects (Vaquer-Sunyer and Duarte 2008; Sturdivant et al. 2014). Thus, as
555 some organisms may be able to tolerate modest and extensive hypoxia but cannot tolerate the
556 most severe periods (Brady et al. 2009), it might be important to trade increased uncertainty for
557 the shorter-term metric. Tradeoffs like this will likely play out in developing most ecological
558 forecasts, where the chosen time frame for prediction is ultimately a function of the ecological
559 target of interest and may include indices for both duration and spatial extent to represent the
560 time-space integration of habitat availability.

561 **Uncertainty characterization** - Quantifying and communicating uncertainty is crucial when
562 forecasts and scenarios are used for environmental decision making (Clark et al. 2001; Harwood
563 and Stokes 2003; Irby and Friedrichs 2019). A rigorous and transparent characterization of
564 forecast uncertainty enables stakeholders and policy makers to a) get a realistic picture of the
565 current state of scientific knowledge of the process being predicted, b) quantitatively evaluate the
566 risk associated with a range of possible future outcomes and make decisions accordingly, and c)
567 prioritize future investments to fill knowledge gaps that are responsible for the largest sources of
568 uncertainty (Pappenberger and Beven 2006; Dietze et al. 2018). The relative magnitude of
569 different error sources provides useful insights on where to focus future research efforts to
570 reduce forecast error (Obenour et al. 2014; Bertani et al. 2016; Del Giudice et al. 2020). The
571 hierarchical approach demonstrated here provides a means to quantify multiple sources of
572 uncertainty, including parameter uncertainty, model prediction error, and HV measurement error.
573 While model predictive performance did not change when incorporating multiple sets of HV
574 estimates, the separate characterization of measurement and prediction error led to wider, but
575 more realistic, prediction intervals (Cressie et al. 2009). The ability to explicitly separate
576 different sources of uncertainty also allowed us to develop different types of predictive intervals,
577 depending on which types of uncertainty are of interest (Fig. 4; See “Management Application”).

578 *Reducing measurement error* - We found that uncertainty associated with HV estimates is an
579 important component of the overall predictive uncertainty (Fig. 4). As a result, efforts to improve
580 HV estimates and reconcile differences across multiple sets of HV estimates have the potential to
581 reduce forecast uncertainty. This is consistent with findings in other systems where a thorough
582 analysis of uncertainty has revealed that accurately capturing temporal dynamics of complex

583 ecological processes such as harmful algal blooms and hypoxia is still a major limitation to
584 reducing forecast error (Del Giudice et al. 2020; Scavia et al. 2020c).

585 While few monitoring programs have the resources needed for the intensive monitoring required
586 to accurately capture metrics such as algal and oxygen dynamics, advances in three-dimensional
587 ecological modeling, space-time geostatistical estimation, and their fusion provide sophisticated
588 interpolations of limited survey data. For example, as computational power increased and three-
589 dimensional ecological models have become more sophisticated, they have been used to both
590 provide insights into oxygen dynamics and integrate point estimates across time and space to
591 generate continuous time series of hypoxia (Bever et al. 2013; Fennel et al. 2016; Katin et al.
592 2019). Geostatistical techniques are also being used to augment discrete monitoring data and
593 generate enhanced estimates of algal blooms and hypoxia dynamics integrated over space and
594 time with quantified uncertainty (Murphy et al. 2011; Obenour et al. 2013; Zhou et al. 2013,
595 2014; Matli et al. 2018; Fang et al. 2019). Matli et al. (2020) combined these two approaches by
596 using output from a three-dimensional ecological model as covariates in their space-time
597 geostatistical analysis for the Gulf of Mexico, reducing prediction uncertainty by 11-40%
598 compared to using measurement alone. As these modeling and geostatistical approaches
599 improve, together with the ever-increasing availability of high-frequency sensors and remote
600 sensing products, the ability to expand beyond the limitations of traditional monitoring will allow
601 for more integrative and accurate ecosystem metrics used in forecast and scenario development.
602 The hierarchical framework presented here also allows for the estimation of separate
603 measurement errors for sets of metrics that are known to be characterized by markedly different
604 measurement uncertainty.

605 *Reducing model error* - Model error results from an incomplete deterministic representation of
606 mechanisms and drivers. This type of uncertainty can be reduced through model improvements
607 that include additional drivers and/or enhance the model's ability to capture biophysical
608 relationships. In our case, a better characterization of the load sources and replacing the
609 calibration target with HV metrics that are less sensitive to short-term weather resulted in
610 improved model performance (Table 1).

611 Considerable inter-annual HV variability remained unexplained (Table 1). This is expected
612 because the relatively simple model does not include other drivers like climate-related variables

613 (Scully 2013; Li et al. 2016; Irby et al. 2018; Du et al. 2018). Models of intermediate complexity
614 that combine the strengths of data assimilation with parsimonious ecological process-based
615 representations have been effective in explaining additional variability in similar systems while
616 retaining the ability to characterize uncertainty (Liu and Scavia 2010; Rucinski et al. 2014;
617 Obenour et al. 2015; Del Giudice et al. 2020). However, adding drivers that help explain
618 additional inter-annual variability but are not reliably forecast at seasonal time scales, as is often
619 the case for weather-related variables, may add substantial uncertainty, or make the model less
620 effective in forecast mode. All ecological forecast models will need to eventually strike a
621 balance between the availability of driver forecasts, model performance, and parsimony.

622 **Value of seasonal forecasts** - Near-term seasonal forecasts benefit scientists and other
623 stakeholders because they generate knowledge on external controls of ecosystems and permit the
624 translation of that knowledge into a prediction with societal value (Testa et al. 2017a; Dietze et
625 al. 2018). Seasonal forecasts relate causes and consequences of ecological conditions and can
626 help raise public awareness of potential controls. Although the initial motivation for an
627 ecological forecast may be to provide operational, quantitative information to support natural
628 resource management, widely-communicated forecasts also engage audiences outside of the
629 resource management community.

630 Public engagement can maintain motivation and build support for improving water quality. The
631 release of seasonal hypoxia forecasts in Chesapeake Bay have facilitated that engagement
632 (Scavia and Bertani 2020), along with periodic updates throughout the summer (Maryland DNR
633 2020), and end-of-year summaries of the yearly severity of hypoxia (VIMS 2020a). Testa et al.
634 (2017a) showed that hypoxia-related media activity increased substantially following initiation
635 of Chesapeake Bay hypoxia forecasts. Articles mentioning forecasts made up 41-56% of all
636 articles related to Chesapeake Bay hypoxia between 2013 and 2015. Similarly, the Gulf of
637 Mexico and Lake Erie annual forecasts each generate hundreds of local and national media
638 reports, resulting in elevated awareness and support for action. Newsletters and websites that
639 supplement the forecasts (e.g., Scavia and Bertani 2020; Rabalais 2020) draw attention to other
640 issues associated with hypoxia, expand discussions around any unexpected factors causing the
641 forecasts to fail, and provide platforms to assess new discoveries while allowing for continuous
642 improvement of the forecast modeling tools.

643 Our efforts also highlight how we can gain scientific insights by building and iteratively
644 revisiting ecological forecast models (Dietze et al. 2018). By routinely evaluating our forecasts
645 against observations and investigating the causes leading to model failure in specific years, we
646 gained critical knowledge that guided refinements of HV metrics and relevant load sources. For
647 example, overprediction of average July HV routinely observed in summers with anomalous
648 weather events (Testa et al. 2017a) led to the exploration of HV metrics that would be less
649 sensitive to transient weather conditions and would thus result in improved model performance
650 (this study). This is only the last of a series of iterations that the model has gone through over the
651 years as new data became available, more forecasts were made, and model performance could be
652 re-assessed. For example, a re-evaluation of model performance with a longer forecasting record
653 led to switching to a more parsimonious model formulation where all parameters are kept
654 constant through time rather than allowed to vary over the years (Evans and Scavia 2011). That
655 work also showed how model parameter values gradually changed and model accuracy and
656 precision improved as individual years were progressively added to the calibration dataset.
657 Results of that study indicated that gradual shifts in parameter estimates over time reflected an
658 apparent increased sensitivity of the system to nutrient loads (Evans and Scavia 2011). Those
659 findings led to the adoption of a moving-window calibration approach for a few years (2010-
660 2014), which was abandoned in 2015 to return to a calibration based on the full dataset (Scavia
661 and Bertani 2020) as new forecast performance indicated excessive sensitivity of the calibration
662 window to years with anomalous weather. By continually updating model calibration as new data
663 became available, we also found that the ratio of both summer average and total annual HV to
664 spring TN load has been increasing in recent years (Appendix S1: Fig. S4). This is consistent
665 with previous research that suggested the Bay became more susceptible to hypoxia over the past
666 35 years (Hagy et al. 2004; Kemp et al. 2005; Murphy et al. 2011). Persistent hypoxia despite N
667 load reductions has been attributed to changes in wind forcing (Scully 2010b), altered spatial
668 patterns of chlorophyll-*a* (Lee et al. 2013; Testa et al. 2018; Wang and Hood 2020), and
669 warming (Du et al. 2018; Ni et al. 2020). These studies point to multiple compounding factors
670 that may be counteracting nutrient reductions and offer hypotheses to test in future applications
671 of our forecast model.

672 In addition, for cases where the same model is used for both seasonal forecasts and scenarios, the
673 track records of the seasonal forecasts provide useful skill assessments and measures of

674 confidence (e.g., Scavia and Bertani 2020; Scavia et al. 2020a,b; Testa et al. 2017a). Examples
675 where the same model has been used for both seasonal and short-term forecasts and scenario
676 planning include hypoxia in the Gulf of Mexico (Scavia et al. 2017), Chesapeake Bay (Irby and
677 Friedrichs 2019, VIMS 2020b), and the Neuse River Estuary (Katin et al. 2019), and harmful
678 algal blooms in Lake Erie (Scavia et al. 2016; Verhamme et al. 2016; Stumpf et al. 2016; Bertani
679 et al. 2016).

680 **Management scenario application** - Unlike other ecological forecasts for the Gulf of Mexico
681 and Lake Erie (GLWQA 2016; Task Force 2016), the original Chesapeake Bay model was not
682 used to guide management decisions, primarily because it was driven only by Susquehanna River
683 loads as opposed to watershed-wide loads. Our analyses demonstrated that driving the model
684 with TN load from all major tributaries and point sources resulted in the best performance for the
685 two metrics that best characterize the system's response to inter-annual variability in loads (Fig.
686 4). This not only corroborates the importance of watershed-wide load reduction strategies as
687 expressed in the Chesapeake Bay TMDL (US EPA 2010), but also makes the revised model
688 more suitable to evaluate those efforts. The Bay's water quality restoration targets are based on
689 spatio-temporal patterns in DO concentrations rather than Bay-wide HV (US EPA 2010), and the
690 resolution of this model prevents it from evaluating those targets directly. However, the model
691 has been useful in tracking progress over time (Testa et al. 2017a). In addition, because the
692 revised model is better connected to watershed-wide restoration efforts, it can now be used (e.g.,
693 Fig. 4) to explore how management actions have influenced hypoxia, how they may influence it
694 in the future, and as an independent line of evidence to support results from the official suite of
695 complex process-based models used by the CBP.

696 Being based on a steady-state solution, the model cannot predict how long it may take to achieve
697 the mean HV expected under a specific management scenario. It is also important to note that
698 scenario predictions may be conservative because our simple model does not account for future
699 changes in biogeochemical processes such as in sediment oxygen demand. Changes in these
700 processes would not influence seasonal forecasts because their impacts would have been
701 accommodated during model calibration. However, such processes may change through time as a
702 result of sustained load reductions. In the short- to mid-term, the accumulation of estuarine
703 nutrients and organic matter is likely to result in a time lag between load reductions and

704 detectable improvements in water quality (Jeppesen et al. 2005; Bocaniov and Scavia 2016);
705 over the long term it is reasonable to expect that substantial and continued load reductions would
706 eventually result in a decrease in oxygen consumption and specifically sediment oxygen demand
707 (Smith and Matisoff 2008; Rucinski et al. 2014). This in turn may lead to additional reductions in
708 HV, although there is substantial uncertainty on how and over what time frames these
709 biogeochemical processes may respond to long-term management actions. Future model
710 enhancements should address this limitation, for example by incorporating parsimonious
711 parameterizations of oxygen consumption processes, similar to what has been done in other
712 systems (Borsuk et al. 2001; Del Giudice et al. 2020; Obenour et al. 2015; Rucinski et al. 2014,
713 2016).

714 Another important consideration when using the model in scenario mode is that it was calibrated
715 to a dataset in which inter-annual variability in loads is largely due to variation in precipitation
716 and hydrology. On the other hand, decreases in loads due to management actions are expected to
717 be mainly associated with decreases in constituent concentrations rather than changes in
718 hydrology. Using the model in scenario mode thus assumes that the relationship between loads
719 and HV observed over the calibration period would hold when changes in loads are due to
720 changes in land management rather than changes in hydrology. Although this is a common
721 underlying assumption of similar relatively simple models used both in forecasting and scenario
722 mode (Obenour et al. 2014; Stumpf et al. 2016; Scavia et al. 2017), the inclusion of separate
723 terms in the model for discharge and nutrient inputs would allow one to explore differences in
724 the system's response to changes in loads due to different factors (Stumpf et al. 2012, Del
725 Giudice et al. 2020).

726 Despite these limitations, some of the characteristics that make this model a useful complement
727 to existing sophisticated three-dimensional hydrodynamic-biogeochemical models of the
728 Chesapeake Bay include a) the ability to seamlessly and readily incorporate new data as they
729 become available and routinely update model calibration in line with an adaptive management
730 approach, b) the fast computation time, which makes it possible to easily evaluate large numbers
731 of management scenarios, and c) the ability to rigorously characterize uncertainty and provide
732 probabilistic predictions. Separating different sources of uncertainty is important because the
733 target of management actions is typically the true, latent state of an ecosystem property (e.g., the

734 true, unknown HV represented by y_i in Eq. 6), which is not affected by measurement error. The
735 portion of the overall model predictive uncertainty that is due to HV measurement error can thus
736 be removed when using the model to answer management questions, thereby leading to narrower
737 prediction intervals (solid gray lines in Fig. 4). In addition to that, different error intervals are
738 relevant to different management questions and uncertainty is generally lower when predicting a
739 long-term average response compared to predictions for individual years (Fig. 4). In our case,
740 when using the model to predict the expected long-term mean HV associated with a given
741 management scenario, stochasticity associated with individual year variability (i.e., model
742 prediction error) is not relevant because it does not influence the expected long-term mean
743 response (Scavia et al. 2020c). However, this source of error should be considered when using
744 the model in forecast mode to accommodate the additional uncertainty arising from forecasting
745 HV in a specific year.

746 **Forecasting best practices** – There is increasing consensus among scientists as to what
747 represent best practices that should be followed when producing, evaluating, and communicating
748 ecological forecasts (Dietze et al. 2018; Harris et al. 2018; White et al. 2019; Carey et al. 2021).
749 Some of those practices have been at the core of this work and we discussed their importance
750 extensively in previous sections, including explicitly accounting for and propagating multiple
751 sources of uncertainty, such as observation and process uncertainty, identifying better predictor
752 variables that are expected to relate to the forecast endpoint, using the model to make both short-
753 and long-term predictions to accommodate the time scales of management decisions while also
754 using short-term forecasts to facilitate evaluation of model performance, and routinely assessing
755 and updating the model with new data (Dietze et al. 2018; Harris et al. 2018; White et al. 2019).
756 Our work also demonstrates the importance of several other proposed best practices. For
757 example, the decrease in the best model's predictive performance when run in blind forecast
758 mode (NSE = 0.47) compared to full calibration mode (NSE = 0.52) confirms the importance of
759 evaluating models through out-of-sample validation approaches, such as hindcasting, to avoid
760 over-optimistic conclusions on forecasting performance (Dietze et al. 2018; Harris et al. 2018;
761 White et al. 2019). We also showed that our model represents an improvement over a baseline
762 model that assumes no changes over time and essentially predicts constant HV (Dietze et al.
763 2018; Harris et al. 2018; White et al. 2019). Finally, loads and DO measurements used to
764 produce our forecasts are made publicly available within 2 and 6-10 months of collection,

765 respectively (Soroka and Blomquist 2020, Chesapeake Bay Program 2020), and past forecasts
766 are archived publicly (Scavia et al. 2019) for retrospective assessment of performance (Dietze et
767 al. 2018; Harris et al. 2018; White et al. 2019).

768 **CONCLUSIONS**

769 We presented an updated and revised version of a long-standing estuarine hypoxia forecasting
770 model. Our revisions focused on some of the most critical challenges and opportunities faced by
771 contemporary ecological forecasting models (Dietze et al. 2018), including a) the adoption of
772 metrics of ecosystem state and anthropogenic pressure that strike an optimal balance between
773 predictability and relevance for management purposes, b) the ability to incorporate multiple data
774 sources within a (Bayesian hierarchical) framework that allows to rigorously separate and
775 propagate different sources of uncertainty, and c) the ability to use the model in scenario mode to
776 probabilistically evaluate the effect of alternative management decisions on future ecosystem
777 state. The model's relative simplicity facilitates an iterative process of model application,
778 evaluation, and enhancement through regular incorporation of updated information and is part of
779 what makes this tool a useful complement to more sophisticated process-based models. Finally,
780 the basic formulation and minimal data needs (DO and TN are among the parameters routinely
781 assessed in water quality monitoring programs) make forecast operations straightforward and
782 transparent and the model itself readily adaptable to other estuarine systems facing similar
783 anthropogenic pressures.

784

785 **ACKNOWLEDGMENTS**

786 The authors would like to thank Jessica Rigelman for assisting with and providing data on point
787 source loads and management scenarios estimated by the Chesapeake Bay Program's watershed
788 model CAST. Richard Tian, Gopal Bhatt, Dave Montali, and Yu-Chen Wang provided numerous
789 helpful discussions and suggestions during model development, analyses, and manuscript
790 preparation. Scavia's contributions were supported in part by USEPA contract EP-C-17-046.
791 Bertani and Murphy's contributions were supported by the USEPA (CBP Technical Support
792 Grant No. 07-5-230480). Friedrichs' contribution to this research was funded by NOAA's
793 National Center for Coastal Ocean Science under award NA16NOS4780207. Testa's
794 contribution to this research was funded by the National Science Foundation (CBET-1360395)

795 and the National Oceanographic and Atmospheric Administration (NA15NOS4780184). This is
796 UMCES Contribution #XXXX and Ref. No. [UMCES] CBL 2XXX-XXX.

Author Manuscript

797 **REFERENCES**

- 798 Ator, S.W., J.D. Blomquist, J.S. Webber, and J.G. Chanat. 2020. Factors driving nutrient trends
799 in streams of the Chesapeake Bay watershed. *Journal of Environmental Quality* 49(4): 812-834.
- 800 Beckage, B., L.J. Gross, and S. Kauffman. 2011. The limits to prediction in ecological systems.
801 *Ecosphere* 2(11): 125.
- 802 Bertani, I., D.R. Obenour, C.E. Steger, C.A. Stow, A.D. Gronewold, and D. Scavia 2016.
803 Probabilistically assessing the role of nutrient loading in harmful algal bloom formation in
804 western Lake Erie. *Journal of Great Lakes Research* 42: 1184-1192.
- 805 Bever, A.J., M.A.M. Friedrichs, C.T. Friedrichs, M.E. Scully, and L.W. Lanerolle. 2013.
806 Combining observations and numerical model results to improve estimates of hypoxic volume
807 within the Chesapeake Bay, USA. *Journal of Geophysical Research: Oceans* 118(10): 4924-
808 4944.
- 809 Bever, A.J., M.A.M. Friedrichs, C.T. Friedrichs, and M.E. Scully. 2018. Estimating hypoxic
810 volume in the Chesapeake Bay using two continuously sampled oxygen profiles. *Journal of*
811 *Geophysical Research: Oceans* 123: 6392-6407.
- 812 Bever, A.J., M.A.M. Friedrichs, and P. St-Laurent. 2021. Real-time environmental forecasts of
813 the Chesapeake Bay: Model setup, improvements, and online visualization. *Environmental*
814 *Modelling and Software* 140: 105036.
- 815 Bocaniov, S., and D. Scavia. 2016. Temporal and spatial dynamics of large lake hypoxia:
816 Integrating statistical and three-dimensional dynamic models to enhance lake management
817 criteria. *Water Resources Research* 52: 4247-4263.
- 818 Boesch, D.F. 2006. Scientific requirements for ecosystem-based management in the restoration
819 of Chesapeake Bay and Coastal Louisiana. *Ecological Engineering* 26(1): 6–26.
- 820 Borsuk, M.E., D. Higdon, C. Stow, and K. Reckhow K. 2001. A Bayesian hierarchical model to
821 predict benthic oxygen demand from organic matter loading in estuaries and coastal zones.
822 *Ecological Modelling* 143: 165–181.
- 823 Brady, D.C., T.E. Targett, and D.M. Tuzzolino. 2009. Behavioral responses of juvenile weakfish
824 (*Cynoscion regalis*) to diel-cycling hypoxia: swimming speed, angular correlation, expected

825 displacement, and effects of hypoxia acclimation. *Canadian Journal of Fisheries and Aquatic*
826 *Sciences* 66: 415-424.

827 Buchheister, A., C.F. Bonzek, J. Gartland, and R.J. Latour. 2013. Patterns and drivers of the
828 demersal fish community of Chesapeake Bay. *Marine Ecology Progress Series* 481: 161–180.

829 Carey, C.C., W.M. Woelmer, M.E. Lofton, R.J. Figueiredo, B.J. Bookout, R.S. Corrigan, V.
830 Daneshmand, A.G. Hounshell, D.W. Howard, A.S.L. Lewis, R.P. McClure, H.L. Wander, N.K.
831 Ward, and R.Q. Thomas. 2021. Advancing lake and reservoir water quality management with
832 near-term, iterative ecological forecasting. *Inland Waters* 1-14.

833 Carpenter, S.R. 2002. Ecological futures: building an ecology of the long now. *Ecology* 83:
834 2069-2083.

835 Chapra, S.C. 1997. *Surface Water-Quality Modeling*. McGraw-Hill, New York.

836 Chesapeake Bay Program. 2017. Chesapeake Assessment and Scenario Tool (CAST) Version
837 2017d. Chesapeake Bay Program Office. Accessed May 2020. <https://cast.chesapeakebay.net/>.

838 Chesapeake Bay Program. 2020. Chesapeake Bay Program Data Hub. Accessed April 2020.
839 <http://www.chesapeakebay.net/data>.

840 Clark, J.S. 2005. Why environmental scientists are becoming Bayesians. *Ecology Letters* 8: 2-14.

841 Clark, J.S., S.R. Carpenter, M. Barber, S. Collins, A. Dobson, J.A. Foley, D.M. Lodge, M.
842 Pascual, R.Jr. Pielke, W. Pizer, C. Pringle, W.V. Reid, K.A. Rose, O. Sala, W.H. Schlesinger,
843 D.H. Wall, and D. Wear. 2001. Ecological forecasts: an emerging imperative. *Science* 293: 657–
844 60.

845 Coreau, A., G. Pinay, J.D. Thompson, P.-O. Cheptou, and L. Mermet. 2009. The rise of research
846 on futures in ecology: rebalancing scenarios and predictions. *Ecology Letters* 12: 1277–1286.

847 Cressie, N., C.A. Calder, J.S. Clark, J.M.V. Hoef, and C.K. Wikle. 2009. Accounting for
848 uncertainty in ecological analysis: the strengths and limitations of hierarchical statistical
849 modeling. *Ecological Applications* 19(3): 553-570.

850 Da, F., M.A.M. Friedrichs, and P. St-Laurent. 2018. Impacts of atmospheric nitrogen deposition
851 and coastal nitrogen fluxes on oxygen concentrations in Chesapeake Bay. *Journal of*
852 *Geophysical Research: Oceans* 123: 5004-5025.

853 Del Giudice, D., V.R.R. Matli, and D.R. Obenour. 2020. Bayesian mechanistic modeling
854 characterizes Gulf of Mexico hypoxia: 1968–2016 and future scenarios. *Ecological Applications*
855 30 (2): e02032.

856 Dietze, M.C., A. Fox, L.M. Beck-Johnson, J.L. Betancourt, M.B. Hooten, C.S. Jarnevich, T.H.
857 Keitt, M.A. Kenney, C.M. Laney, L.G. Larsen, H.W. Loescher, C.K. Lunch, B.C. Pijanowski,
858 J.T. Randerson, E.K. Read, A.T. Tredennick, R. Vargas, K.C. Weathers, and E.P. White. 2018.
859 Iterative near-term ecological forecasting: Needs, opportunities, and challenges. *Proceedings of*
860 *the National Academy of Sciences* 115(7): 1424-1432.

861 Du, J., J. Shen, K. Park, Y.-P. Wang, and X. Yu. 2018. Worsened physical condition due to
862 climate change contributes to the increasing hypoxia in Chesapeake Bay. *Science of The Total*
863 *Environment* 630: 707-717.

864 EFI. 2020. Ecological Forecasting Initiative. Forecasts to understand, manage, and conserve
865 ecosystems. Webpage. Accessed November 2020. <https://ecoforecast.org>.

866 Eshleman, K.N., R.D. Sabo, and K.M. Kline. 2013. Surface Water Quality Is Improving due to
867 Declining Atmospheric N Deposition. *Environmental Science and Technology* 47(21): 12193–
868 12200.

869 Evans, M.R., M. Bithell, S.J. Cornell, S.R.X. Dall, S. Diaz, S. Emmott, B. Ernande, V. Grimm,
870 D.J. Hodgson, S.L. Lewis, G.M. Mace, M. Morecroft, A. Moustakas, E. Murphy, T. Newbold,
871 K.J. Norris, O. Petchey, M. Smith, J.M.J. Travis, and T.G. Benton. 2013 Predictive systems
872 ecology. *Proceedings of the Royal Society B* 280: 20131452.

873 Evans, M.A., and D. Scavia 2011. Forecasting hypoxia in the Chesapeake Bay and Gulf of
874 Mexico: Model accuracy, precision, and sensitivity to ecosystem change. *Environmental*
875 *Research Letters* 6: 015001.

876 Fang, S., D. Del Giudice, D. Scavia, C.E. Binding, T.B. Bridgeman, J.D. Chaffin, M.A. Evans, J.
877 Guinness, T.H. Johengen, and D.R. Obenour. 2019. A space-time geostatistical model for
878 probabilistic estimation of harmful algal bloom biomass and areal extent. *Science of the Total*
879 *Environment* 695: 133776.

880 Feng, Y., S.F. DiMarco, and G.A. Jackson. 2012. Relative role of wind forcing and riverine
881 nutrient input on the extent of hypoxia in the northern Gulf of Mexico. *Geophysical Research*
882 *Letters* 39: L09601, doi:10.1029/2012GL051192.

883 Fennel, K., A. Laurent, R. Hetland, D. Justic', D.S. Ko, J. Lehrter, M. Murrell, L. Wang, L. Yu,
884 and W. Zhang. 2016. Effects of model physics on hypoxia simulations for the northern Gulf of
885 Mexico: A model intercomparison. *Journal of Geophysical Research: Oceans* 121: 5731–5750.

886 Gelman, A., and J. Hill. 2007. Data analysis using regression and multilevel/hierarchical models.
887 Cambridge University Press, New York.

888 Gimenez, O., S.T. Buckland, B.J.T. Morgan, N. Bez, S. Bertrand, R. Choquet, S. Dray, M-P.
889 Etienne, R. Fewster, F. Gosselin, B. Merigot, P. Monestiez, J.M. Morales, F. Mortier, F. Munoz,
890 O. Ovaskainen, S. Pavoine, R. Pradel, F.M. Schurr, L. Thomas, W. Thuiller, V. Trenkel, P. de
891 Valpine, and E. Rexstad. 2014. Statistical ecology comes of age. *Biology Letters* 10(12):
892 20140698.

893 GLWQA. 2016. Great Lakes Water Quality Agreement. The United States and Canada adopt
894 phosphorus load reduction targets to combat Lake Erie algal blooms.
895 <https://binational.net/2016/02/22/finalptargets-ciblesfinalesdep/>

896 Gneiting, T., and M. Katzfuss. 2014. Probabilistic forecasting. *Annual Review of Statistics and*
897 *Its Application* 1: 125-151.

898 Goodrich, D.M., W.C. Boicourt, P. Hamilton, and D.W. Pritchard. 1987. Wind-induced
899 destratification in Chesapeake Bay. *Journal of Physical Oceanography* 17(12): 2232-2240.

900 Gurbisz, C., and W.M. Kemp. 2014. Unexpected resurgence of a large submersed plant bed in
901 Chesapeake Bay: analysis of time series data. *Limnology and Oceanography* 59(2): 482–494.

902 Hagy, J.D., W.R. Boynton, C.W. Keefe, and K.V. Wood. 2004. Hypoxia in Chesapeake Bay,
903 1950-2001: long-term change in relation to nutrient loading and river flow. *Estuaries* 4 (4): 634–
904 658.

905 Harris, D.J., S.D. Taylor, and E.P. White. 2018. Forecasting biodiversity in breeding birds using
906 best practices. *PeerJ* 6: e4278.

907 Harwood, J., and K. Stokes. 2003. Coping with uncertainty in ecological advice: lessons from
908 fisheries. *Trends in Ecology and Evolution* 18(12): 617-622.

909 Hirsch, R.M., D.L. Moyer, and S.A. Archfield. 2010. Weighted regression on time, discharge,
910 and season (WRTDS), with an application to Chesapeake Bay river inputs. *Journal of the*
911 *American Water Resources Association* 46: 857–880.

912 Hofman, J.M., D.G. Goldstein, and J. Hullman. 2020. How visualizing inferential uncertainty
913 can mislead readers about treatment effects in scientific results. *Proceedings of the 2020 CHI*
914 *Conference on Human Factors in Computing Systems*.

915 Irby, I.D., and M.A.M. Friedrichs. 2019. Evaluating confidence in the impact of regulatory
916 nutrient reduction on Chesapeake Bay water quality. *Estuaries and Coasts* 42: 16-32.

917 Irby, I.D., M.A.M. Friedrichs, F. Da, and K.E. Hinson. 2018. The Competing Impacts of Climate
918 Change and Nutrient Reductions on Dissolved Oxygen in Chesapeake Bay. *Biogeosciences* 15:
919 2649–2668.

920 Irby, I.D., M.A.M. Friedrichs, C.T. Friedrichs, A.J. Bever, R.R. Hood, L.W.J. Lanerolle, M. Li,
921 L. Linker, M.E. Scully, K. Sellner, J. Shen, J. Testa, H. Wang, P. Wang, and M. Xia. 2016.
922 Challenges associated with modeling low-oxygen waters in Chesapeake Bay: A multiple model
923 comparison. *Biogeosciences* 13: 2011-2028.

924 Jeppesen, E., M. Søndergaard, J.P. Jensen, K.E. Havens, O. Anneville, L. Carvalho, M.F.
925 Coveney, R. Deneke, M.T. Dokulil, B. Foy, D. Gerdeaux, S.E. Hampton, S. Hilt, K. Kangur, J.
926 Kohler, E.H.H.R. Lammens, T.L. Lauridsen, M. Manca, M.R. Miracle, B. Moss, P. Noges, G.
927 Persson, G. Phillips, R. Portielje, S. Romo, C.L. Schelske, D. Straile, I. Tatrai, E. Willen, and M.
928 Winder. 2005. Lake responses to reduced nutrient loading - An analysis of contemporary long-
929 term data from 35 case studies. *Freshwater Biology* 50: 1747–1771.

930 Johnson-Bice, S.M., J.M. Ferguson, J.D. Erb, T.D. Gable, and S.K. Windels. 2020. Ecological
931 forecasts reveal limitations of common model selection methods: predicting changes in beaver
932 colony densities. *Ecological Applications*: e02198.

933 Jordan, A., F. Krüger, and S. Lerch. 2019. Evaluating Probabilistic Forecasts with scoringRules.
934 *Journal of Statistical Software* 90(12): 1–37.

935 Katin, A., D. Del Giudice, and D.R. Obenour. 2019. Modeling biophysical controls on hypoxia
936 in a shallow estuary using a Bayesian mechanistic approach. *Environmental Modelling &*
937 *Software* 120: 104491.

938 Kemp, W.M., W.R. Boynton, J.E. Adolf, D.F. Boesch, W.C. Boicourt, G. Brush, J.C. Cornwell,
939 T.R. Fisher, P.M. Glibert, J.D. Hagy, L.W. Harding, E.D. Houde, D.G. Kimmel, W.D. Miller,
940 R.I.E. Newell, M.R. Roman, E.M. Smith, J.C. Stevenson. 2005. Eutrophication of Chesapeake
941 Bay: historical trends and ecological interactions. *Marine Ecology Progress Series* 303:1-29.

942 Lee, Y.J., W.R. Boynton, M. Li, and Y. Li. 2013. Role of late winter-spring wind influencing
943 summer hypoxia in Chesapeake Bay. *Estuaries and Coasts* 36: 683-696.

944 Lefcheck, J.S., R.J. Orth, W.C. Dennison, D.J. Wilcox, R.R. Murphy, J. Keisman, C. Gurbisz,
945 M. Hannam, J.B. Landry, K.A. Moore, C.J. Patrick, J. Testa, D.E. Weller, and R.A. Batiuk.
946 2018. Long-term nutrient reductions lead to the unprecedented recovery of a temperate coastal
947 region. *Proceedings of the National Academy of Sciences* 115(14): 3658-3662.

948 Li, M., Y.J. Lee, J.M. Testa, Y. Li, W. Ni, W.M. Kemp, and D.M. Di Toro. 2016. What drives
949 interannual variability of hypoxia in Chesapeake Bay: Climate forcing versus nutrient loading?
950 *Geophysical Research Letters* 43: 2127– 2134.

951 Linker, L.C., R.A. Batiuk, G.W. Shenk, and C.F. Cerco. 2013. Development of the Chesapeake
952 Bay watershed total maximum daily load allocation. *Journal of the American Water Resources*
953 *Association* 49(5): 986–1006.

954 Liu, Y., G.B. Arhonditsis, C.A. Stow, and D. Scavia. 2011. Predicting the hypoxic-volume in
955 Chesapeake Bay with the Streeter Phelps model: a Bayesian approach. *Journal of the American*
956 *Water Resources Association* 1(6): 1348–1363.

957 Liu, Y., and D. Scavia. 2010. Analysis of the Chesapeake Bay Hypoxia Regime Shift: Insights
958 from Two Simple Mechanistic Models. *Estuaries and Coasts* 33: 629-639.

959 Lunn, D.J., A. Thomas, N. Best, and D. Spiegelhalter. 2000. WinBUGS—A Bayesian modelling
960 framework: Concepts, structure, and extensibility. *Statistics and Computing* 10: 325–337.

961 Luo, Y.Q., K. Ogle, C. Tucker, S.F. Fei, C. Gao, S. LaDeau, J.S. Clark, and D.S. Schimel. 2011.
962 Ecological forecasting and data assimilation in a data-rich era. *Ecological Applications* 21(5):
963 1429–1442.

964 Maryland DNR. 2020. Chesapeake Bay Hypoxia Reports. Webpage. Accessed November 2020.
965 <https://dnr.maryland.gov/waters/bay/Pages/Hypoxia-Reports.aspx>.

966 Matheson, J.E., and R.L. Winkler. 1976. Scoring rules for continuous probability distributions.
967 *Management Science* 22(10): 1087-1096.

968 Matli, V.R.R., S. Fang, J. Guinness, N.N. Rabalais, J.K. Craig, and D.R. Obenour. 2018. Space-
969 Time Geostatistical Assessment of Hypoxia in the Northern Gulf of Mexico *Environmental*
970 *Science and Technology* 52: 12484–12493.

971 Matli, V.R.R., A. Laurent, K. Fennel, K. Craig, J. Krause, and D.R. Obenour. 2020. Fusion-
972 Based Hypoxia Estimates: Combining Geostatistical and Mechanistic Models of Dissolved
973 Oxygen Variability. *Environmental Science and Technology* 54: 13016–13025.

974 Mistiaen, J.A., I.E. Strand, and D. Lipton. 2003. Effects of environmental stress on blue crab
975 (*Callinectes sapidus*) harvests in Chesapeake Bay tributaries. *Estuaries* 26(2): 316–322.

976 Modig, H., and E. Ólafsson. 1998. Responses of Baltic benthic invertebrates to hypoxic events.
977 *Journal of Experimental Marine Biology and Ecology* 229: 133-148.

978 Moriarty, J.M., M.A.M. Friedrichs, and C.K. Harris. 2020. Seabed resuspension in the
979 Chesapeake Bay: Implications for biogeochemical cycling and hypoxia. *Estuaries and Coasts*.

980 Mouquet, N., Y. Lagadeuc, V. Devictor, L. Doyen, A. Duputie, D. Eveillard, D. Faure, E.
981 Garnier, O. Gimenez, P. Huneman, F. Jabot, P. Jarne, D. Joly, R. Julliard, S. Kefi, G. J. Kergoat,
982 S. Lavorel, L. Le Gall, L. Meslin, S. Morand, X. Morin, H. Morlon, G. Pinay, R. Pradel, F. M.
983 Schurr, W. Thuiller, and M. Loreau. 2015. Predictive ecology in a changing world. *Journal of*
984 *Applied Ecology* 52: 1293-1310.

985 Murphy, R.R., W.M. Kemp, and W.P. Ball. 2011. Long-term trends in Chesapeake Bay seasonal
986 hypoxia, stratification, and nutrient loading. *Estuaries and Coasts* 34: 1293–1309.

987 NASA. 2020. Ecological Forecasting. Strengthening Ecosystems. Webpage. Accessed
988 November 2020. <https://appliedsciences.nasa.gov/what-we-do/ecological-forecasting>.

989 Ni, W., M. Li, A.C. Ross, and R.G. Najjar. 2020. Large Projected decline in dissolved oxygen in
990 a eutrophic estuary due to climate change. *Journal of Geophysical Research: Oceans* 124: 8271–
991 8289.

- 992 NOAA. 2020. NOAA Ecological Forecasting. Predicting human health and coastal economies
993 with early warnings. Webpage. Accessed November 2020.
994 <https://oceanservice.noaa.gov/ecoforecasting/>
- 995 NOAA GLERL. 2020. Experimental Lake Erie Hypoxia Forecast. Webpage. Accessed
996 November 2020.
997 https://www.glerl.noaa.gov/res/HABs_and_Hypoxia/hypoxiaWarningSystem.html.
- 998 North Carolina Sea Grant. 2020. Midsummer Neuse River Forecast Shows Greater Potential for
999 Fish Kills. Webpage. Accessed November 2020.
1000 <https://ncseagrant.ncsu.edu/currents/2020/06/midsummer-neuse-river-forecast-shows-greater->
1001 [potential-for-fish-kills/](https://ncseagrant.ncsu.edu/currents/2020/06/midsummer-neuse-river-forecast-shows-greater-potential-for-fish-kills/).
- 1002 Obenour, D.R., A.D. Gronewold, C.A. Stow, and D. Scavia. 2014. Using a Bayesian hierarchical
1003 model to improve Lake Erie cyanobacteria bloom forecasts. *Water Resources Research* 50:
1004 7847–7860.
- 1005 Obenour D.R., A.M. Michalak, and D. Scavia. 2015. Assessing biophysical controls on Gulf of
1006 Mexico hypoxia through probabilistic modeling. *Ecological Applications* 25: 492–505.
- 1007 Obenour, D.R., D. Scavia, N.N. Rabalais, R.E. Turner, and A.M. Michalak. 2013. Retrospective
1008 analysis of midsummer hypoxic area and volume in the northern Gulf of Mexico, 1985–2011.
1009 *Environmental Science and Technology* 47(17): 9808–9815.
- 1010 Pappenberger, F., and K. J. Beven. 2006. Ignorance is bliss: Or seven reasons not to use
1011 uncertainty analysis. *Water Resources Research* 42: W05302.
- 1012 Pappenberger, F., M.-H. Ramos, H.L. Cloke, F. Wetterhall, L. Alfieri, K. Bogner, A. Mueller,
1013 and P. Salamon. 2015. How do I know if my forecasts are better? Using benchmarks in
1014 hydrological ensemble prediction. *Journal of Hydrology* 522: 697-713.
- 1015 Payne, M.R., A.J. Hobday, B.R. MacKenzie, D. Tommasi, D.P. Dempsey, S. Fassler, A.C.
1016 Haynie, R. Ji, G. Liu, P.D. Lynch, D. Matei, A.K. Miesner, K.E. Mills, K.O. Strand, and E.
1017 Villarino. 2017. Lessons from the first generation of marine ecological forecast products.
1018 *Frontiers in Marine Science* 4: 289.
- 1019 Petchey, O.L., M. Pontarp, T.M. Massie, S. Kéfi, A. Ozgul, M. Weilenmann, G.M. Palamara, F.
1020 Altermatt, B. Matthews, J.M. Levine, D.Z. Childs, B.J. McGill, M.E. Schaepman, B. Schmid, P.

1021 Spaak, A.P. Beckerman, F. Pennekamp, and I.S. Pearse. 2015. The ecological forecast horizon,
1022 and examples of its uses and determinants. *Ecology Letters* 18(7): 597-611.

1023 Thomas, R.Q., R.J. Figueiredo, V. Daneshmand, B.J. Bookout, L.K. Puckett, and C.C. Carey.
1024 2020. A near-term iterative forecasting system successfully predicts reservoir hydrodynamics
1025 and partitions uncertainty in real time. *Water Resources Research* 56(11): e2019WR026138.

1026 R Core Team. 2018. R: A language and environment for statistical computing. R Foundation for
1027 Statistical Computing, Vienna.

1028 Rabalais, N.N. 2020. Gulf of Mexico Hypoxia. <https://gulfhypoxia.net/>

1029 Raftery, A.E. 2016. Use and communication of probabilistic forecasts. *Statistical Analysis and*
1030 *Data Mining: The ASA Data Science Journal* 9(6): 397-410.

1031 Ross, A.C., C.A. Stock, K.W. Dixon, M.A.M. Friedrichs, R.R. Hood, M. Li, K. Pegion, V. Saba,
1032 and G.A. Vecchi. 2020. Estuarine forecasts at daily weather to subseasonal time scales. *Earth*
1033 *and Space Science* 7: e2020EA001179.

1034 Rucinski, D., D. Scavia, J. DePinto, and D. Beletsky. 2014. Lake Erie's hypoxia response to
1035 nutrient loads and meteorological variability. *Journal of Great Lakes Research* 40(3): 151-161.

1036 Rucinski, D., J. DePinto, D. Beletsky, and D. Scavia. 2016. Modeling hypoxia in the Central
1037 Basin of Lake Erie under potential phosphorus load reduction scenarios. *Journal of Great Lakes*
1038 *Research* 42: 1206-1211.

1039 Scavia, D., N.N. Rabalais, R.E. Turner, D. Justic, and W. Wiseman Jr. 2003. Predicting the
1040 response of Gulf of Mexico Hypoxia to variations in Mississippi River Nitrogen Load.
1041 *Limnology and Oceanography* 48(3): 951-956.

1042 Scavia, D., M.A. Evans, and D.R. Obenour. 2013. A scenario and forecast model for Gulf of
1043 Mexico hypoxic area and volume. *Environmental Science and Technology* 47:10423–10428.

1044 Scavia, D., and I. Bertani. 2020. Chesapeake Bay Hypoxic Volume Forecasts. June 7, 2020.
1045 Available at: [http://scavia.seas.umich.edu/wp-content/uploads/2020/10/2020-Chesapeake-Bay-](http://scavia.seas.umich.edu/wp-content/uploads/2020/10/2020-Chesapeake-Bay-forecast_EndOfSummer.pdf)
1046 [forecast_EndOfSummer.pdf](http://scavia.seas.umich.edu/wp-content/uploads/2020/10/2020-Chesapeake-Bay-forecast_EndOfSummer.pdf)

- 1047 Scavia, D., Y-C., Wang, and D.R. Obenour. 2020a. Lake Erie Harmful Algal Bloom Forecast.
1048 June 7, 2020. Available at: [http://scavia.seas.umich.edu/wp-content/uploads/2020/07/2020-
LakeErieBloomForecastRelease.pdf](http://scavia.seas.umich.edu/wp-content/uploads/2020/07/2020-
1049 LakeErieBloomForecastRelease.pdf)
- 1050 Scavia, D., I. Bertani, C. Long, D.R. Obenour, and Y-C. Wang. 2020b. Gulf of Mexico Hypoxia
1051 Forecast. June 7, 2020. Available at: [http://scavia.seas.umich.edu/wp-
content/uploads/2020/08/2020-Gulf-of-Mexico-Hypoxic-Forecast.pdf](http://scavia.seas.umich.edu/wp-
1052 content/uploads/2020/08/2020-Gulf-of-Mexico-Hypoxic-Forecast.pdf)
- 1053 Scavia, D., I. Bertani, C. Long, and Y. Wang. 2019. Chesapeake Bay Hypoxic Volume
1054 Forecasts. June 7, 2019. Available at: [http://scavia.seas.umich.edu/wp-
content/uploads/2019/06/2019-Chesapeake-Bay-forecast.pdf](http://scavia.seas.umich.edu/wp-
1055 content/uploads/2019/06/2019-Chesapeake-Bay-forecast.pdf)
- 1056 Scavia, D., I. Bertani, D.R. Obenour, R.E. Turner, D.R. Forrest, and A. Katin. 2017. Ensemble
1057 modeling informs hypoxia management in the northern Gulf of Mexico. *Proceedings of the
1058 National Academy of Sciences* 114: 8823-8828.
- 1059 Scavia, D., J.V. DePinto, and I. Bertani. 2016. A Multi-model approach to evaluating target
1060 phosphorus loads for Lake Erie. *Journal of Great Lakes Research* 42: 1139-1150.
- 1061 Scavia, D., E.L.A. Kelly, and J.D. Hagy. 2006. A simple model for forecasting the effects of
1062 nitrogen loads on Chesapeake Bay hypoxia. *Estuaries and Coasts* 29 (4): 674–684.
- 1063 Scavia, D., Y-C. Wang, D.R. Obenour, A. Apostel, S.J. Basile, M.M. Kalcic, C.J. Kirchhoff, L.
1064 Miralha, R.L. Muenich, and A.L. Steiner. 2020c. Quantifying uncertainty cascading from
1065 climate, watershed, and lake models in harmful algal bloom predictions. *Science of the Total
1066 Environment*: 143487.
- 1067 Schindler, D.E., and R. Hilborn. 2015. Prediction, precaution, and policy under global change.
1068 *Science* 347(6225): 953-954.
- 1069 Scully, M.E. 2010a. Wind Modulation of Dissolved Oxygen in Chesapeake Bay. *Estuaries and
1070 Coasts* 33: 1164–1175.
- 1071 Scully, M.E. 2010b. The importance of climate variability to wind-driven modulation of hypoxia
1072 in Chesapeake Bay. *Journal of Physical Oceanography* 40(6): 1435-1440.
- 1073 Scully, M.E. 2013. Physical controls on hypoxia in Chesapeake Bay: A numerical modeling
1074 study. *Journal of Geophysical Research: Oceans* 118: 1239-1256.

- 1075 Shenk, G.W., and L.C. Linker. 2013. Development and application of the 2010 Chesapeake Bay
1076 Watershed total maximum daily load model. *Journal of the American Water Resources*
1077 *Association* 49 (5): 1042–1056.
- 1078 Salon, S., G. Cossarini, G. Bolzon, L. Feudale, P. Lazzari, A. Teruzzi, C. Solidoro, A. Crise.
1079 2019. Novel metrics based on Biogeochemical Argo data to improve the model uncertainty
1080 evaluation of the CMEMS Mediterranean marine ecosystem forecasts. *Ocean Sci.*, 15, 997–1022,
1081 2019 <https://doi.org/10.5194/os-15-997-2019>
- 1082 Smith, D.A., and G. Matisoff. 2008. Sediment oxygen demand in the central basin of Lake Erie.
1083 *Journal of Great Lakes Research* 34(4): 731–744.
- 1084 Soroka, A.M., and D.J. Blomquist. 2020. Nitrogen flux estimates in support of Chesapeake Bay
1085 Hypoxia and Anoxia forecasts, 1985-2020: U.S. Geological Survey data release,
1086 <https://doi.org/10.5066/P9QU1DWS>.
- 1087 Stow, C.A., and D. Scavia. 2009. Modeling hypoxia in the Chesapeake Bay: ensemble estimation
1088 using a Bayesian hierarchical model. *Journal of Marine Systems* 76(1-2): 244-250.
- 1089 Streeter, H.W., and E.B. Phelps. 1925. A Study in the Pollution and Natural Purification of the
1090 Ohio River, III Factors Concerning the Phenomena of Oxidation and Reaeration. US Public
1091 Health Service, Public Health Bulletin No. 146, Feb 1925 Reprinted by US PHEW, PHA 1958.
- 1092 Sturdivant, S.K., M.J. Brush, and R.J. Diaz. 2013. Modeling the Effect of Hypoxia on
1093 Macrobenthos Production in the Lower Rappahannock River, Chesapeake Bay, USA. *Plos One*
1094 8: e84140.
- 1095 Sturdivant, S.K., R.J. Díaz, R.Llansó, and D.M. Dauer. 2014. Relationship between Hypoxia and
1096 Macrobenthic Production in Chesapeake Bay. *Estuaries and Coasts* 37 (5): 1219-1232.
- 1097 Stumpf R.P., T.T. Wynne, D.B. Baker, G.L. Fahnenstiel. 2012. Interannual Variability of
1098 Cyanobacterial Blooms in Lake Erie. PLoS ONE 7(8): e42444.
1099 [doi:10.1371/journal.pone.0042444](https://doi.org/10.1371/journal.pone.0042444)
- 1100 Stumpf, R.P., L.T. Johnson, T.T. Wynne, and D.B. Baker. 2016. Forecasting annual
1101 cyanobacterial bloom biomass to inform management decisions in Lake Erie. *Journal of Great*
1102 *Lakes Research* 42(6): 1174–1183.

1103 Sturtz, S., U. Ligges, and A.E. Gelman. 2005. R2WinBUGS: A package for running WinBUGS
1104 from R. *Journal of Statistical Software* 12 (3): 1–16.

1105 Task Force. 2016. Mississippi River/Gulf of Mexico Watershed Nutrient Task Force. Looking
1106 forward: The strategy of the federal members of the Hypoxia Task Force (Mississippi River/Gulf
1107 of Mexico Watershed Nutrient Task Force, Washington, DC). Available at [https://www.
1108 epa.gov/sites/production/files/2016-12/documents/federal_strategy_updates_12.2.16.pdf](https://www.epa.gov/sites/production/files/2016-12/documents/federal_strategy_updates_12.2.16.pdf).

1109 Testa, J.M., Y. Li, Y.J. Lee, M. Li, D.C. Brady, D.M.D. Toro, and W.M. Kemp. 2014.
1110 Quantifying the effects of nutrient loading on dissolved O₂ cycling and hypoxia in Chesapeake
1111 Bay using a coupled hydrodynamic-biogeochemical model. *Journal of Marine Systems* 139: 139-
1112 158.

1113 Testa, J.M., J.B. Clark, W.C. Dennison, E.C. Donovan, A.W. Fisher, W. Ni, M. Parker, D.
1114 Scavia, S.E. Spitzer, A.M. Waldrop, V.M.D. Vargas, and G. Ziegler. 2017a. Ecological
1115 forecasting and the science of hypoxia in Chesapeake Bay. *Bioscience* 67 (7): 614–626.

1116 Testa, J.M., Y. Li, Y.J. Lee, M. Li, D.C. Brady, D.M.D. Toro, and W.M. Kemp. 2017b.
1117 Modeling physical and biogeochemical controls on dissolved oxygen in Chesapeake Bay:
1118 Lessons learned from simple and complex approaches. In *Modeling Coastal Hypoxia -
1119 Numerical Simulations of Patterns, Controls and Effects of Dissolved Oxygen Dynamics*, ed. D.
1120 Justic, K. Rose, R. Hetland and K. Fennel. Cham, Switzerland: Springer.

1121 Testa, J.M., R.R. Murphy, D.C. Brady, and W.M. Kemp. 2018. Nutrient- and Climate-Induced
1122 Shifts in the Phenology of Linked Biogeochemical Cycles in a Temperate Estuary. *Frontiers in
1123 Marine Science* 5: 114.

1124 Turner, R.E., N.N. Rabalais, and D. Justić. 2012. Predicting summer hypoxia in the northern
1125 Gulf of Mexico: redux. *Marine Pollution Bulletin* 64: 319-324.

1126 US EPA. 2003. Ambient Water Quality Criteria for Dissolved Oxygen, Water Clarity and
1127 Chlorophyll a for the Chesapeake Bay and its Tidal Tributaries Rep., 343 pp, U.S.
1128 Environmental Protection Agency Region III, Chesapeake Bay Program Office, Annapolis, MD.

- 1129 US EPA. 2010. Chesapeake Bay total maximum daily load for nitrogen, phosphorus and
1130 sediment. Available at: [https://www.epa.gov/chesapeake-bay-tmdl/chesapeake-bay-tmdl-
document](https://www.epa.gov/chesapeake-bay-tmdl/chesapeake-bay-tmdl-
1131 document)
- 1132 Valette-Silver, N. and D. Scavia. 2003. Ecological forecasting: New tools for coastal and marine
1133 ecosystem management. NOAA Technical Memorandum NOS NCCOS 1, 116 pp.
1134 [http://scavia.seas.umich.edu/wp-
content/uploads/2009/11/noaa_ecological_forecasting_book1.pdf](http://scavia.seas.umich.edu/wp-
1135 content/uploads/2009/11/noaa_ecological_forecasting_book1.pdf)
- 1136 Vaquer-Sunyer, R. and C.M. Duarte. 2008. Thresholds of hypoxia for marine biodiversity.
1137 *Proceedings of the National Academy of Sciences*. 105(40): 15452-15457.
- 1138 Verhamme, E., T. Redder, D. Schlea, J. Grush, J. Bratton, and J. DePinto. 2016. Development of
1139 the Western Lake Erie Ecosystem Model (WLEEM): application to connect phosphorus loads to
1140 cyanobacteria biomass. *Journal of Great Lakes Research* 42(6): 1193–1205.
- 1141 VIMS. 2020a. Chesapeake Bay Dead-Zone Report Card. November 2020. Available at:
1142 https://www.vims.edu/research/topics/dead_zones/forecasts/report_card/index.php.
- 1143 VIMS. 2020b. Chesapeake Bay Hypoxia Forecast. Webpage. Accessed November 2020.
1144 https://www.vims.edu/research/topics/dead_zones/forecasts/cbay/index.php.
- 1145 Wang, J., and R.R. Hood. 2020. Modeling the origin of the particulate organic matter flux to the
1146 hypoxic zone of Chesapeake Bay in early summer. *Estuaries and Coasts* doi:10.1007/s12237-
1147 020-00806-0.
- 1148 White, E.P., G.M. Yenni, S.D. Taylor, E.M. Christensen, E.K. Bledsoe, J.L. Simonis, and S.M.
1149 Ernest. 2019. Developing an automated iterative near-term forecasting system for an ecological
1150 study. *Methods in Ecology and Evolution* 10(3): 332-344.
- 1151 WIP 2020. Chesapeake Bay Watershed Implementation Plans. Chesapeake Bay Program.
1152 https://www.chesapeakebay.net/what/programs/watershed_implementation. Accessed May 20
1153 2020.
- 1154 Zhang, H., L. Boegman, D. Scavia, and D.A. Culver. 2016. Spatial distributions of external and
1155 internal phosphorus loads in Lake Erie and their impacts on phytoplankton and water quality.
1156 *Journal of Great Lakes Research* 42: 1212-1227.

1157 Zhang, Q., R.R. Murphy, R. Tian, M.K. Forsyth, E.M. Trentacoste, J. Keisman, and P.J. Tango.
1158 2018. Chesapeake Bay's water quality condition has been recovering: insights from a multimetric
1159 indicator assessment of thirty years of tidal monitoring data. *Science of the Total Environment*
1160 637–638: 1617–1625.

1161 Zhou, Y., D.R. Obenour, D. Scavia, T.H. Johengen, and A.M. Michalak. 2013. Spatial and
1162 temporal trends in Lake Erie hypoxia, 187–2007. *Environmental Science and Technology* 47(2):
1163 899–905.

1164 Zhou, Y., D. Scavia, and A.M. Michalak. 2014. Nutrient loading and meteorological conditions
1165 explain interannual variability of hypoxia in the Chesapeake Bay. *Limnology and Oceanography*
1166 59: 373-374.

1167

1168

1169

1170 **Tables**

1171

1172 **Table 1** - Best performing model for each HV metric. NSE = Nash-Sutcliffe Efficiency, r^2 =
1173 square of the correlation coefficient between observed and predicted values, RMSE = root mean
1174 square error, MAE = mean absolute error, RSTDE = residual standard error, Coverage =
1175 percentage of the observations used in calibration that fall within the 95% prediction intervals,
1176 CRPS = Continuous Ranked Probability Score, CRPS score = CRPS skill score (see text for
1177 definition), Sus = Susquehanna, Pot = Potomac, PS = point sources. Results for September HV
1178 not shown because no model resulted in $NSE > 0$. Three Average July models have the same
1179 NSE. For comparison, performance of the previous model version (driven by Jan-May
1180 Susquehanna River loads and predicting Average July HV) is also reported, together with
1181 performance of the two best models predicting Average July and Total Annual HV with
1182 Susquehanna loads only.

1183

HV metric	Load Sources	Load Period	NSE	r²	RMSE	MAE	RSTDE	Coverage	CRPS	CRPS score
June	All tributaries	Mar-Jun	0.25	0.30	1.75	1.45	1.81	100%	1.02	0.12
July	Sus + Pot + PS	Oct-May	0.29	0.30	2.38	1.82	2.46	94%	1.35	0.20
July	Sus + Pot + PS	Nov-Jun	0.29	0.29	2.39	1.82	2.47	97%	1.35	0.19
July	All tributaries + PS	Nov-May	0.29	0.29	2.39	1.78	2.52	94%	1.36	0.19
August	All tributaries + PS	Jan-Jun	0.22	0.24	1.63	1.30	1.69	97%	0.93	0.20
Summer	All tributaries + PS	Jan-Jun	0.40	0.43	1.01	0.81	1.04	94%	0.57	0.26
Annual	All tributaries + PS	Jan-Jun	0.52	0.52	123	96	130	94%	68.12	0.36
July	Sus	Jan-May	0.14	0.18	2.62	2.08	2.68	97%	1.49	0.10
July	Sus	Dec-Jun	0.23	0.24	2.49	1.98	2.60	97%	1.42	0.14

Annual	Sus	Jan-May	0.28	0.37	150	113	156	97%	82.17	0.22
--------	-----	---------	------	------	-----	-----	-----	-----	-------	------

1184

1185

1186 **Table 2** - Total annual and summer average HVs (mean and 95% credible intervals) predicted
 1187 under different total nitrogen (TN) load scenarios. For details on each scenario see text.

Scenario	Jan-Jun TN Load (kg/day)	Total Annual HV (95% CI) (km ³ *days)	Summer Average HV (95% CI) (km ³)
1985 FN	486713	930 (840-1005)	7.2 (6.5-7.8)
2018 FN	350360	770 (640-870)	5.9 (4.9-6.5)
2020 No Action	564932	995 (910-1085)	7.8 (7.2-8.4)
WIP3 Actual	285570	660 (480-785)	4.9 (3.8-5.9)
WIP3 Planning Targets	274250	635 (440-785)	4.7 (3.4-5.6)

1188

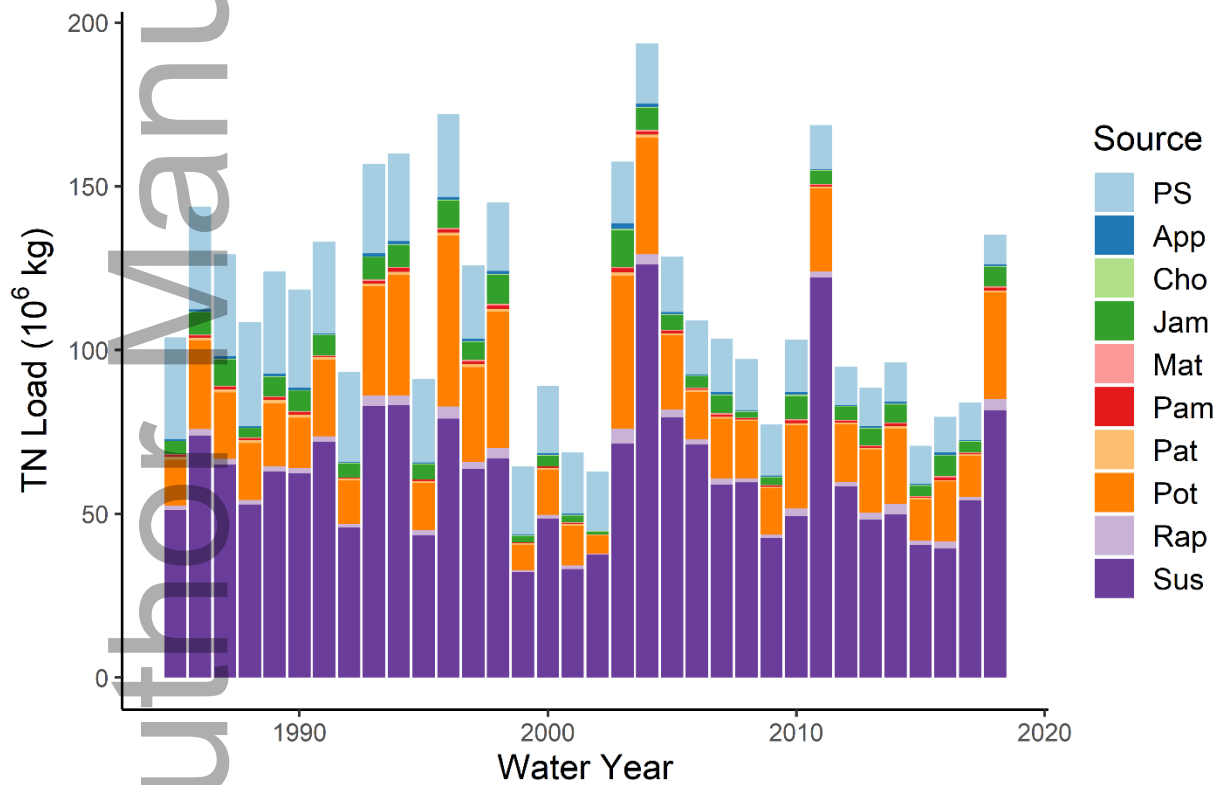
1189 **FIGURE CAPTIONS**

1190 Fig. 1 - Annual total nitrogen (TN) loads from nine tributaries (Sus: Susquehanna; Rap:
 1191 Rappahannock; Pot: Potomac; Pat: Patuxent; Pam: Pamunkey; Mat: Mattaponi; App:
 1192 Appomattox; Jam: James; Cho: Choptank) and point sources downstream from the tributary
 1193 monitoring stations (PS). Point source data for Jul-Sep 2018 are partial. Water year: Oct-Sep.

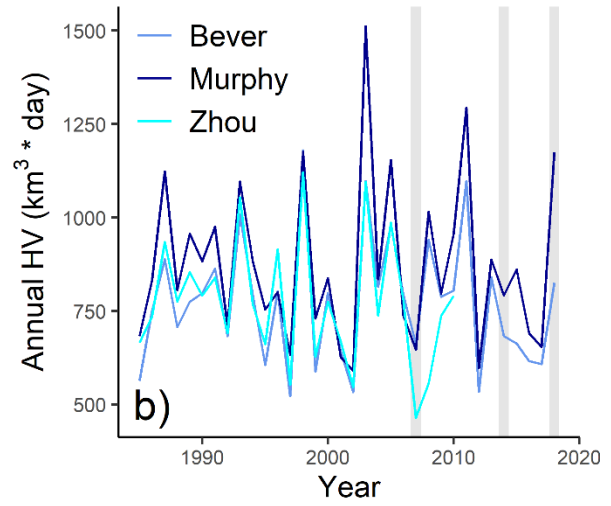
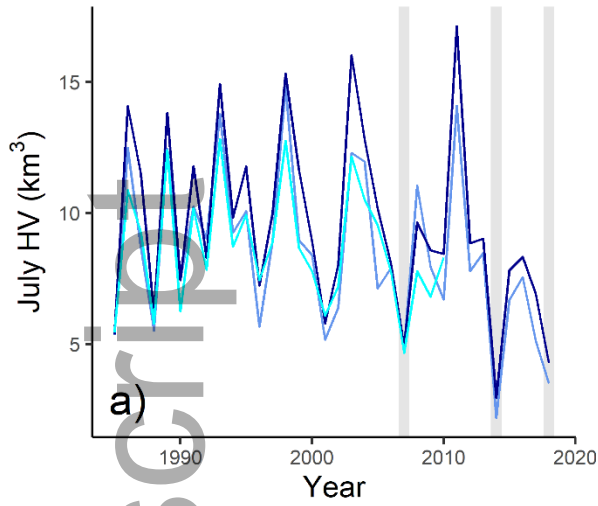
1194 Fig. 2 - Average July (a) and total annual (b) hypoxic volumes (HVs) estimated using three
 1195 different interpolation methods over 1985-2018. Zhou estimates are available only through 2010.
 1196 Shaded areas mark years when weather events disrupted hypoxia shortly before the July cruises.

1197 Fig. 3 - Observed vs. predicted total annual (a) and summer average (b) HV for the model
 1198 calibrated to three sets of HV estimates simultaneously. The gray bars represent 95% predictive
 1199 intervals accounting for model prediction error, HV measurement error, and parameter
 1200 uncertainty. The 1:1 line is shown in black for reference.

1201 Fig. 4 - Response curves for total annual (a) and summer average (b) HV vs. average Jan-Jun
 1202 load from all tributaries and point sources. The response curves were generated using models
 1203 calibrated to three sets of HV estimates simultaneously (means of the three sets of estimates
 1204 shown as circles for the years 1985-1994, squares for the years 1995-2004 and diamonds for the
 1205 years 2005-2018). HV estimates are colored according to the corresponding average Jan-Jun
 1206 flow from all tributaries. Shaded area: 95% credible intervals (accounting for parameter
 1207 uncertainty); solid gray lines: 95% prediction intervals (accounting for parameter uncertainty and
 1208 prediction error); dashed gray lines: 95% prediction intervals (accounting for parameter
 1209 uncertainty, prediction error and HV estimation error). Dashed vertical and horizontal lines
 1210 indicate the mean HV expected under different management scenarios after averaging out year-
 1211 to-year variability in hydrology (see main text for a description of each scenario).



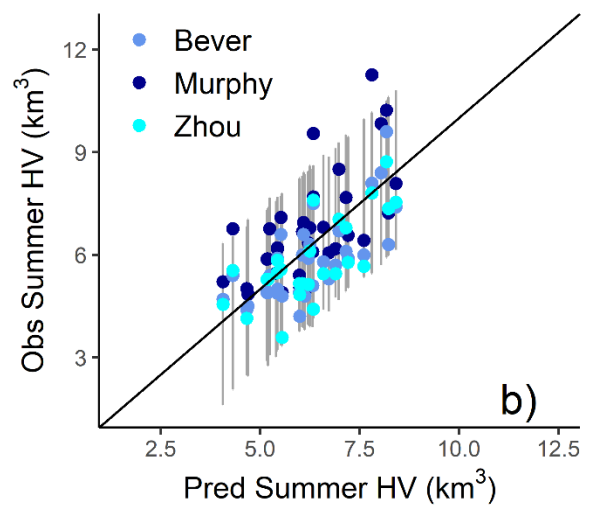
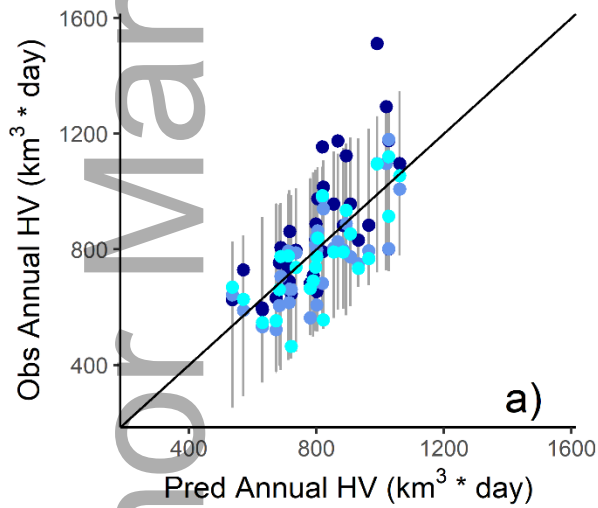
1212
 1213 Fig. 1
 1214



1215

1216 Fig. 2

1217



1218

1219 Fig. 3

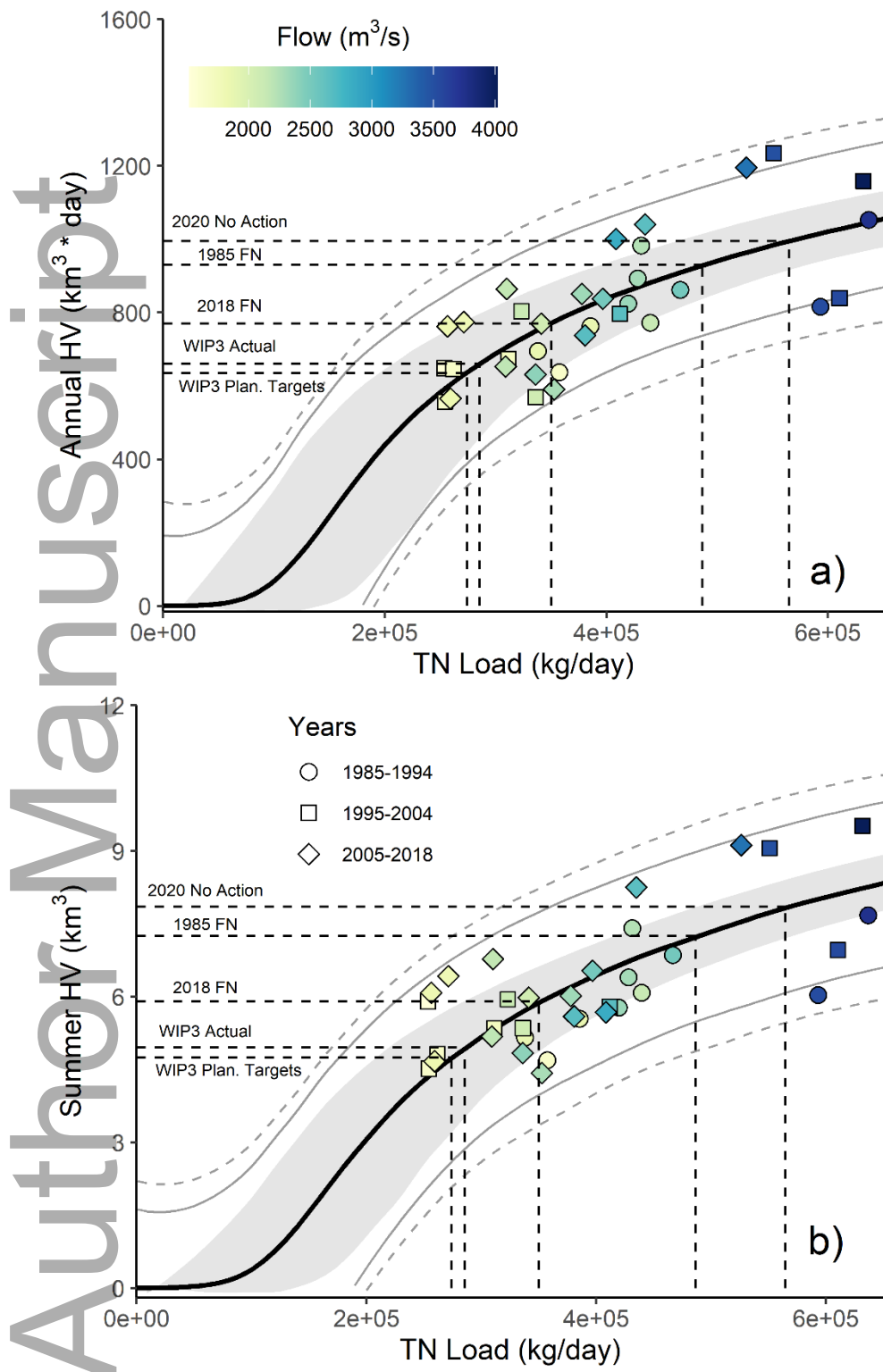
1220

1221

1222

1223

1224



1225

1226 Fig. 4